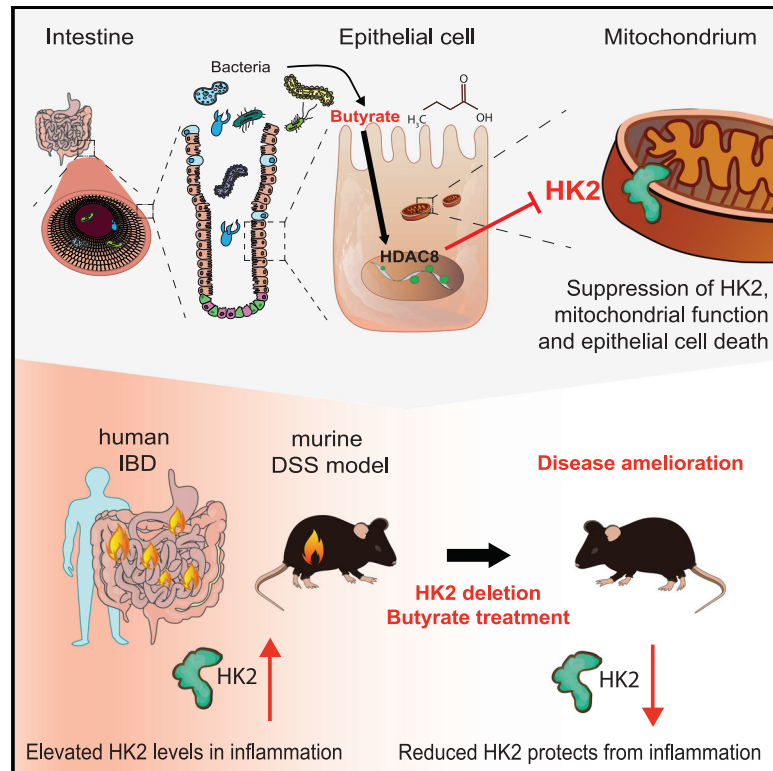


# Cell Metabolism

## Microbial regulation of hexokinase 2 links mitochondrial metabolism and cell death in colitis

### Graphical abstract



### Authors

Finn Hinrichsen, Jacob Hamm, Magdalena Westermann, ..., Fredrik Bäckhed, Philip Rosenstiel, Felix Sommer

### Correspondence

f.sommer@ikmb.uni-kiel.de

### In brief

Hinrichsen and Hamm et al. report that HK2 and its microbial regulation control intestinal homeostasis. Using genetic and gnotobiotic mouse models, they reveal that deleting epithelial HK2 protects against colitis by suppressing cell death and altering mitochondrial function. Further, the microbial metabolite butyrate downregulates HK2, thereby providing protection from colitis.

### Highlights

- Loss of epithelial HK2 protects against acute intestinal inflammation
- Ablation of HK2 suppresses cell death and dysregulates mitochondrial function
- The microbiome regulates HK2 expression via SCFAs targeting HDAC8
- The SCFA butyrate ameliorates intestinal inflammation by downregulating HK2



## Article

# Microbial regulation of hexokinase 2 links mitochondrial metabolism and cell death in colitis

Finn Hinrichsen,<sup>1,15</sup> Jacob Hamm,<sup>1,15</sup> Magdalena Westermann,<sup>1</sup> Lena Schröder,<sup>1</sup> Kensuke Shima,<sup>2</sup> Neha Mishra,<sup>1</sup> Alesia Walker,<sup>3</sup> Nina Sommer,<sup>1</sup> Kenneth Klischies,<sup>1</sup> Daniela Prasse,<sup>4</sup> Johannes Zimmermann,<sup>5</sup> Sina Kaiser,<sup>1</sup> Dora Bordoni,<sup>1</sup> Antonella Fazio,<sup>1</sup> Georgios Marinou,<sup>5</sup> Georg Laue,<sup>1</sup> Simon Imm,<sup>1</sup> Valentina Tremaroli,<sup>6</sup> Marijana Basic,<sup>7</sup> Robert Häsler,<sup>1,8</sup> Ruth A. Schmitz,<sup>4</sup> Stefan Krautwald,<sup>9</sup> Andrea Wolf,<sup>10</sup> Bärbel Stecher,<sup>11,12</sup> Philippe Schmitt-Kopplin,<sup>3</sup> Christoph Kaleta,<sup>5</sup> Jan Rupp,<sup>2</sup> Fredrik Bäckhed,<sup>6,13,14</sup> Philip Rosenstiel,<sup>1,16</sup> and Felix Sommer<sup>1,16,17,\*</sup>

<sup>1</sup>Institute of Clinical Molecular Biology, University of Kiel, 24105 Kiel, Germany

<sup>2</sup>Department of Infectious Diseases and Microbiology, University of Lübeck, 23538 Lübeck, Germany

<sup>3</sup>Research Unit Analytical BioGeoChemistry, Helmholtz Zentrum München, German Research Centre for Environmental Health (GmbH), 85764 Neuherberg, Germany

<sup>4</sup>Institute of General Microbiology, University of Kiel, 24118 Kiel, Germany

<sup>5</sup>Institute of Experimental Medicine, University of Kiel, 24105 Kiel, Germany

<sup>6</sup>The Wallenberg Laboratory, Department of Molecular and Clinical Medicine, University of Gothenburg, 41345 Gothenburg, Sweden

<sup>7</sup>Institute for Laboratory Animal Science, Hannover Medical School, 30625 Hannover, Germany

<sup>8</sup>Department of Dermatology and Allergy, University Hospital Schleswig-Holstein, 24105 Kiel, Germany

<sup>9</sup>Department of Nephrology and Hypertension, University Hospital Schleswig-Holstein, 24105 Kiel, Germany

<sup>10</sup>Department of Biomedical Sciences, Cedars-Sinai Medical Center, Los Angeles, CA 90048, USA

<sup>11</sup>Max von Pettenkofer Institute of Hygiene and Medical Microbiology, Ludwig-Maximilians-University of Munich, 80336 Munich, Germany

<sup>12</sup>German Center for Infection Research (DZIF), partner site LMU Munich, Munich Germany

<sup>13</sup>Department of Clinical Physiology, Sahlgrenska University Hospital, Gothenburg, Sweden

<sup>14</sup>Novo Nordisk Foundation Center for Basic Metabolic Research, Faculty of Health and Medical Sciences, University of Copenhagen, 2200, Copenhagen, Denmark

<sup>15</sup>These authors contributed equally

<sup>16</sup>Senior author

<sup>17</sup>Lead contact

\*Correspondence: [f.sommer@ikmb.uni-kiel.de](mailto:f.sommer@ikmb.uni-kiel.de)

<https://doi.org/10.1016/j.cmet.2021.11.004>

## SUMMARY

Hexokinases (HK) catalyze the first step of glycolysis limiting its pace. HK2 is highly expressed in gut epithelium, contributes to immune responses, and is upregulated during inflammation. We examined the microbial regulation of HK2 and its impact on inflammation using mice lacking HK2 in intestinal epithelial cells ( $Hk2^{\Delta IEC}$ ).  $Hk2^{\Delta IEC}$  mice were less susceptible to acute colitis. Analyzing the epithelial transcriptome from  $Hk2^{\Delta IEC}$  mice during colitis and using HK2-deficient intestinal organoids and Caco-2 cells revealed reduced mitochondrial respiration and epithelial cell death in the absence of HK2. The microbiota strongly regulated HK2 expression and activity. The microbially derived short-chain fatty acid (SCFA) butyrate repressed HK2 expression via histone deacetylase 8 (HDAC8) and reduced mitochondrial respiration in wild-type but not in HK2-deficient Caco-2 cells. Butyrate supplementation protected wild-type but not  $Hk2^{\Delta IEC}$  mice from colitis. Our findings define a mechanism how butyrate promotes intestinal homeostasis and suggest targeted HK2-inhibition as therapeutic avenue for inflammation.

## INTRODUCTION

Hexokinases (HK) catalyze the first step of glycolysis and thereby limit the rate of this fundamental biological process. HK2 is considered the prototypic inducible isoform of all HK family members as it can be upregulated by various environmental factors and signaling pathways, e.g., during inflammation and in inflammatory bowel disease (IBD) (Everts et al., 2014; Perrin-Coccon et al., 2018; Taman et al., 2018). In addition to its metabolic function, HK2 acts as a receptor for bacterial cell wall compo-

nents (Wolf et al., 2016) and has been suggested to counteract mitochondria-mediated cell death (Machida et al., 2006). Chemical inhibition of HK impairs immune cell activation and promotes infection by *Listeria monocytogenes* in immune cells (Li et al., 2019), whereas hyperglycemia and high glycolytic flux have been associated with an increased risk of enteric infection in intestinal epithelial cells (Thaiss, et al., 2018). However, complete ablation of HK2 is embryonically lethal (Heikkinen, et al., 1999). In the intestine, *Hk2* is predominantly expressed by intestinal epithelial cells (IECs) (Sommer et al., 2015; Tabula Muris et al.,



2018). Therefore, we aimed to investigate whether selective ablation of HK2 in IECs alters epithelial function during intestinal inflammation. Here we show that (1) loss of HK2 in IECs protects from dextran sodium sulfate (DSS)-induced colitis by decreasing inflammation-induced epithelial cell death and that (2) specific bacterial species and the microbial metabolite butyrate ameliorate colitis by repressing *Hk2* expression.

## RESULTS

### Loss of HK2 in the intestinal epithelium protects from colitis

To determine the role of epithelial HK2 for intestinal inflammation, we generated *Hk2<sup>fl/fl</sup>-Villin::Cre<sup>+</sup>* mice lacking HK2 specifically in IECs, hereinafter referred to as *Hk2<sup>ΔIEC</sup>* mice. We used littermate *Hk2<sup>fl/fl</sup>* mice, hereinafter referred to as WT mice, as controls. Unchallenged *Hk2<sup>ΔIEC</sup>* mice did not display any major inflammatory or metabolic phenotype except for an improved glucose tolerance (Figure S1), compared to littermate controls. However, when *Hk2<sup>ΔIEC</sup>* mice and their WT littermates were challenged with DSS to induce intestinal inflammation, *Hk2<sup>ΔIEC</sup>* mice lost significantly less weight compared to WT littermates (Figure 1A). The disease activity index (DAI)—a measure of intestinal inflammation comprised of weight loss, stool consistency, and fecal blood occurrence—confirmed the ameliorated disease course in *Hk2<sup>ΔIEC</sup>* mice (Figure 1B). Additionally, *Hk2<sup>ΔIEC</sup>* mice displayed lower serum levels of the pro-inflammatory cytokine KC/CXCL1 as measured by ELISA (Figure 1C). Histological evaluation of H&E-stained colon sections demonstrated a reduced score consisting of transmural inflammation, crypt hyperplasia, epithelial injury, and polymorphonuclear and mononuclear cell infiltrates in *Hk2<sup>ΔIEC</sup>* mice (Figure 1D). In WT mice, HK2 levels increased during the course of colitis (Figure 1E; Figure S2I). We therefore investigated whether *Hk2* expression is dysregulated in patients suffering from intestinal inflammation by evaluating expression data from mucosal biopsies of patients that had been made available alongside published articles on public databases in processed format (read counts). In pediatric IBD *HK2* was significantly upregulated in biopsies of IBD patients in comparison to healthy controls (Haberman et al., 2014; Mari-gorta et al., 2017). Both pediatric Crohn's disease (CD) and ulcerative colitis (UC) patients showed an upregulated expression of *HK2*; however in CD patients *HK2* expression was more enhanced (Figures 1F and 1G). Similarly, adult patients suffering from IBD and non-IBD-colitis (NIC) generally showed a higher *HK2* expression than healthy patients (Figure 1H; Häsl er et al., 2017; Quraishi et al., 2020; Weiser et al., 2018). A significantly higher *HK2* expression was observed for UC (Quraishi et al., 2020) and in the inflamed mucosa of CD patients in comparison to healthy controls (Häsl er et al., 2017). Interestingly, also patients with primary sclerosing cholangitis (PSC) showed a higher expression of *Hk2* in IECs indicating a possible correlation between *Hk2* and IBD-associated diseases (Figure 1I; Quraishi et al., 2020).

### Ablation of HK2 protects from cell death and dysregulates mitochondrial function

To decipher the molecular mechanisms protecting *Hk2<sup>ΔIEC</sup>* mice from intestinal inflammation, we isolated IECs from WT and

*Hk2<sup>ΔIEC</sup>* mice on day 0 (baseline), 3 (early inflammation) and 7 (late inflammation) from an independent acute DSS experiment and performed RNA sequencing. While we did not find any differentially expressed genes on day 3, we identified 420 differentially expressed genes on day 7 in comparison between WT and *Hk2<sup>ΔIEC</sup>* mice (Figure S3 and Table S1). Gene Ontology (GO) analysis of these differentially expressed genes revealed a downregulation of genes involved in cell death signaling and regulation of mitochondrial membrane permeability in *Hk2<sup>ΔIEC</sup>* mice (Figure 1J). We confirmed a reduction of cell death in *Hk2<sup>ΔIEC</sup>* mice by terminal deoxynucleotidyl transferase dUTP nick end labeling (TUNEL)-staining of colon sections from day 3 and day 7 of the experiment. In accordance with our transcriptomics data, we found fewer TUNEL-positive cells in the tip compartment of colonic crypts in *Hk2<sup>ΔIEC</sup>* mice at day 3 and 7, indicating less cell death (Figure 1K). This finding coincides with the spatial expression profile of HK2, which is mainly restricted to the colonic epithelial tip (Figure S1N).

To further study the molecular processes involved in HK2-dependent protection from inflammation, we generated intestinal organoids derived from *Hk2<sup>ΔIEC</sup>* and WT mice and investigated their response to stimulation with tumor necrosis factor (TNF). Western blot analysis demonstrated higher HK2 levels upon TNF stimulation (Figure 2A). Organoids derived from *Hk2<sup>ΔIEC</sup>* mice exhibited lower levels of cleaved Caspase 3 and Poly(ADP-Ribose)-Polymerase 1 (PARP1), markers for mitochondria-related types of cell death, compared to WT organoids upon TNF stimulation. This data therefore supported reduced levels of cell death in the absence of HK2 under inflammatory conditions. Furthermore, our transcriptome data suggested dysregulated mitochondrial function as a consequence of loss of HK2. We therefore performed metabolic flux analysis using Seahorse technology. As the 3D structure of organoids limits their use in this assay, we generated a Caco-2 cell clone lacking HK2 using the CRISPR Cas9 system, hereinafter named Caco-2<sup>ΔHk2</sup>. We assessed glycolytic flux by measuring the extracellular acidification rate (ECAR) upon addition of glucose to induce glycolytic flux, oligomycin to stress the glycolytic reserve, and 2-desoxyglucose to inhibit glycolysis. Throughout the entire experiment, we did not observe any significant changes between Caco-2<sup>ΔHk2</sup> and Caco-2<sup>WT</sup> cells, indicating that ablation of HK2 did not affect glycolytic function (Figure 2B). We also measured the basal oxygen consumption rate (OCR), which comprises both mitochondrial and non-mitochondrial oxygen consumption. Interestingly, we discovered significantly lower basal mitochondrial respiration as well as a drastically lower maximal mitochondrial respiration in Caco-2<sup>ΔHk2</sup> cells compared to Caco-2<sup>WT</sup> cells (Figure 2C), indicating impairment of the mitochondrial electron transport chain (ETC) in Caco-2<sup>ΔHk2</sup> cells. Importantly, various groups reported that activities of the ETC including Complex I and the regulation of mitochondrial permeability are correlated in cellular metabolism (Beutner et al., 2017; Bonora and Pinton, 2014; Briston et al., 2017; Li et al., 2012; Weiss et al., 2003). We therefore screened our transcriptome data for differentially expressed genes that are involved in regulation of mitochondrial membrane permeability. Indeed, we observed a downregulation of genes that play a role in the regulation of mitochondrial permeability in HK2-deficient conditions using transcriptome

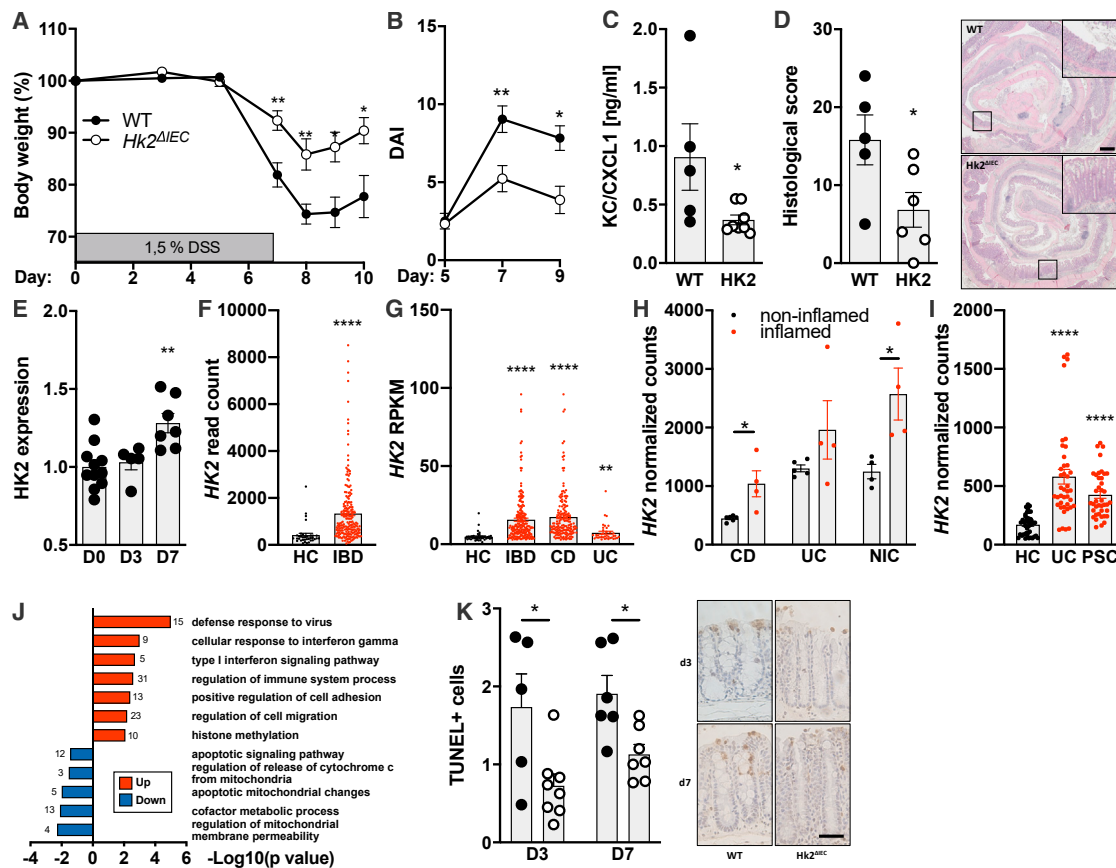


**Figure 1. Loss of HK2 in the intestinal epithelium protects from colitis**

(A) Body weight loss of WT and *Hk2*<sup>ΔIEC</sup> mice lacking HK2 in intestinal epithelial cells during DSS-induced colitis. \*p < 0.05 and \*\*p < 0.01 WT versus *Hk2*<sup>ΔIEC</sup> mice using two-way ANOVA.

(B) Disease activity index (DAI) consisting of stool consistency, fecal blood occurrence, and body weight loss. \*p < 0.05 and \*\*p < 0.01 WT versus *Hk2*<sup>ΔIEC</sup> mice using two-way ANOVA.

(C) KC/CXCL1 (pro-inflammatory cytokine) levels in serum of WT and *Hk2*<sup>ΔIEC</sup> mice as determined by ELISA. \*p < 0.05 using Mann-Whitney U test.

(D) Histological score of H&E-stained sections from colon of WT and *Hk2*<sup>ΔIEC</sup> mice including representative images of the experimental groups. The scale bar represents 500 μm. \*p < 0.05 using Mann-Whitney U test.

(E) Relative HK2 protein expression during the course of DSS-induced colitis in colon epithelium of WT mice as determined by immunohistochemistry. \*\*p < 0.01 versus D0 using one-way ANOVA.

(F–I) *Hk2* expression is dysregulated in intestinal mucosal biopsies of pediatric (F and G) and adult (H and I) patients with inflammatory bowel disease (IBD) irrespective of disease type Crohn's disease (CD) or ulcerative colitis (UC). Note that the y-axes in the panels show both raw and normalized read counts. (F) *Hk2* expression in healthy controls (HC, n = 60) or treatment-naive pediatric IBD patients (n = 210). Data from Margorta et al., 2017. \*\*\*\*p value < 0.0001 using Mann-Whitney U test. (G) *Hk2* expression in HC (n = 42) or treatment-naive pediatric patients with CD (n = 174), UC (n = 38) or combined as IBD (n = 212). Data from Haberman et al., 2014. \*\*p < 0.01 and \*\*\*\*p < 0.0001 using one-way ANOVA. (H) *Hk2* expression was determined in inflamed and non-inflamed intestinal mucosal biopsies from adult patients with CD, UC, or non-IBD Colitis (NIC) by RNA-seq. n = 4–6 per group. \*p < 0.05. (I) *Hk2* expression in HC (n = 40) and adult patients with UC (n = 40) or PSC (n = 40). Data from Quraishi et al., 2020. \*\*\*\*p < 0.0001 using one-way ANOVA.

(J) Gene ontology terms enriched in up- and downregulated genes in transcriptomes of colonic IEC isolated from *Hk2*<sup>ΔIEC</sup> compared to WT mice sacrificed on day 7 of DSS colitis.

(K) Fewer apoptotic cells per colon crypt in *Hk2*<sup>ΔIEC</sup> mice as determined by TUNEL assay including representative images. The scale bar represents 50 μm. \*p < 0.05 using two-way ANOVA. Data are presented as means ± SEM.

sequencing and GO analysis (Figures 1J and S3). Particularly, we observed a downregulation of mRNA levels of *Ppif* (peptidyl-prolyl cis-trans isomerase), encoding for a main component of the mitochondrial permeability transition pore (MPTP) in IECs of *Hk2*<sup>ΔIEC</sup> mice on day 7 of colitis (Figure 2D). PPIF coordinates mitochondrial permeability and metabolism (Baines et al., 2005; Basso et al., 2005; Nakagawa et al., 2005; Schinzel et al., 2005) and has been suggested to directly interact with

HK2 to suppress cell death (Machida et al., 2006). To validate our *in vivo* findings and transcriptome data, we stimulated Caco-2<sup>ΔHk2</sup> and Caco-2<sup>WT</sup> cells with TNF and IL17A (Straus, 2013) as well as with IFN-β to induce inflammatory responses and cell death. Indeed, *Ppif* expression was downregulated under both conditions (Figure 2E). Based on our findings and since PPIF interacts with HK2 (Machida et al., 2006) and *Ppif*<sup>-/-</sup> mice are less susceptible to colitis (Zhu et al., 2016),

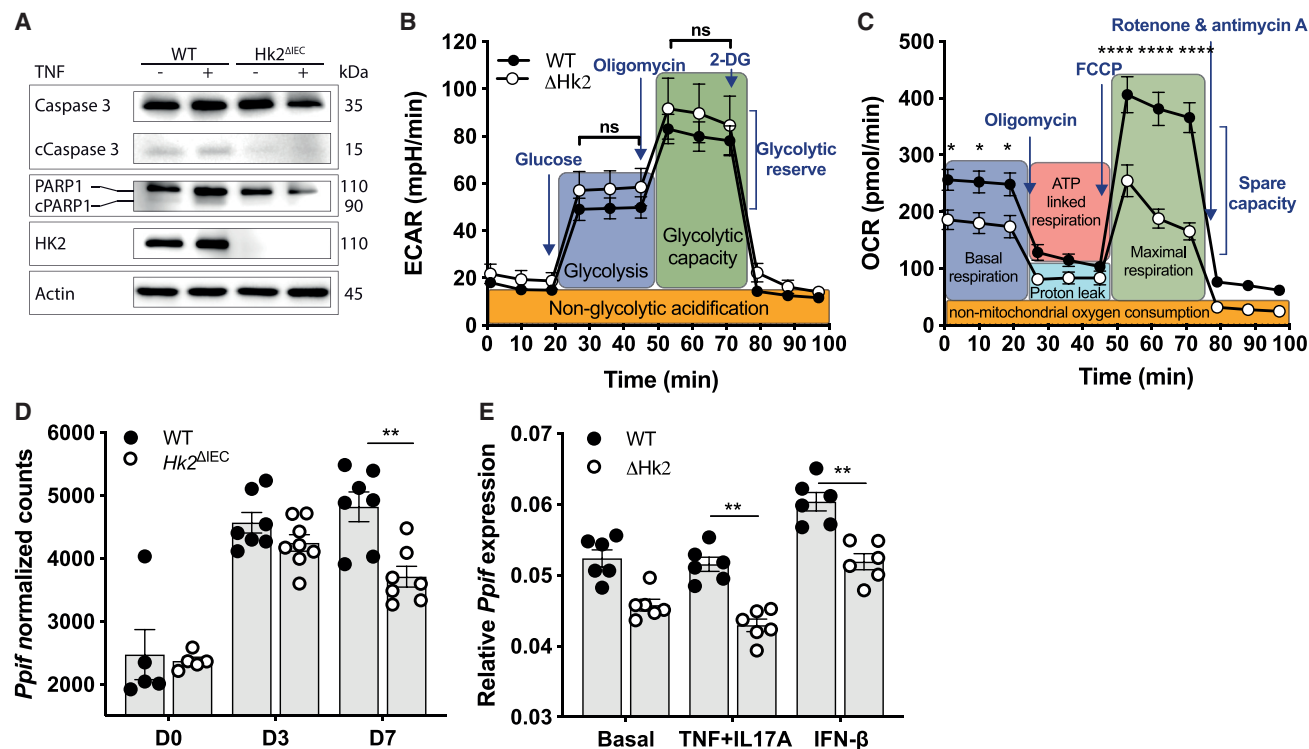


**Figure 2. Dysregulated mitochondrial function in response to loss of HK2**

(A) Western blot analysis protein lysates of intestinal organoids raised from WT and *Hk2*<sup>ΔIEC</sup> mice after stimulation with 100 ng/mL TNF for 24 h. (B and C) Metabolic analysis of Caco-2<sup>WT</sup> and *Hk2*-deficient Caco-2<sup>ΔHk2</sup> cells using the Seahorse XF analyzer. \**p* < 0.05 and \*\*\*\**p* < 0.0001 WT versus  $\Delta Hk2$  using two-way ANOVA. (B) The extracellular acidification rate (ECAR) reflects the glycolytic flux (ns = non-significant). (C) The oxygen consumption rate (OCR) indicates mitochondrial respiration, which was impaired due to loss of HK2. \**p* < 0.05, \*\*\*\**p* < 0.0001. (D) Epithelial *Ppif* expression was downregulated in *Hk2*<sup>ΔIEC</sup> compared to WT mice during the course of DSS-induced colitis (days 0, 3, and 7) as determined by RNA sequencing (normalized read counts). \*\**p* < 0.01 WT versus *Hk2*<sup>ΔIEC</sup> using two-way ANOVA. (E) Reduced *Ppif* expression as measured by qPCR in Caco-2<sup>ΔHk2</sup> compared to Caco-2<sup>WT</sup> cells upon 24 h stimulation with TNF (100 ng/mL) and IL17A (50 ng/mL) or with IFN- $\beta$  (50 ng/mL) to induce inflammation. \*\**p* < 0.01 WT versus  $\Delta Hk2$  using two-way ANOVA. Data are presented as means  $\pm$  SEM.

we propose that mechanistically the HK2-dependent protection from intestinal inflammation could potentially be mediated by lower levels of PPIF and a subsequent decrease in MPTP opening and mitochondrial membrane permeability.

### The intestinal microbiome regulates HK2 expression

Dysregulated host-microbiota interactions are a key element of intestinal inflammation (Sommer and Bäckhed, 2013). By comparing the transcriptomes of intestinal epithelial cell fractions isolated from germ-free (GF) and conventionally raised (CR) C57BL6/J mice (Sommer et al., 2015), we identified *Hk2* as significantly upregulated by the presence of a complex microbial community. *Hk2* expression was specifically induced in the epithelial tips of both ileum and colon by the microbiota (Figure 3A). Upon colonization of GF mice with a normal microbiota *Hk2* expression increased and normalized to that of CR mice, demonstrating that the intestinal microbiota stimulates *Hk2* expression (Figure 3B). However, although we were able to show a distinct effect of the microbiota on *Hk2* expression, ablation of HK2 in IECs in turn did not impact the composition of the intestinal microbiota as assessed by 16S rRNA amplicon sequencing under basal unchallenged conditions (Figure S4). Next, we investigated how the microbiota regulates epithelial

*Hk2* expression, specifically whether specific bacterial species modulate *Hk2* expression. To that end, we colonized GF C57BL6/J mice with either single bacterial species or minimal consortia—namely the Altered Schaedler Flora (ASF) (Dewhirst, et al., 1999) and the Oligo Mouse Microbiota (OMM) (Brugiroux et al., 2016). Both minimal microbial consortia readily induced *Hk2* expression to a similar level as observed in CR mice (Figure 3C). Mono-colonization with the Gram-negative bacterium *Bacteroides thetaiotaomicron* was also able to induce *Hk2* expression, whereas the Gram-negative bacterium *Escherichia coli* and the Gram-positive bacterium *Bifidobacterium longum* did not alter *Hk2* mRNA levels (Figure 3C). Together, these data suggested a specific interaction between bacterial features and epithelial cells rather than general principles such as recognition of lipopolysaccharide or peptidoglycan as a mechanism regulating HK2 expression. We thus next aimed to disentangle the effects of individual OMM bacteria to identify potential candidate principles regulating *Hk2* expression. To that end, we stimulated Caco-2 cells with sterile-filtered culture supernatants of the individual species of the OMM consortium. We identified *Enterococcus faecalis* KB1 as the key inducer among this minimal microbiota (Figure 3D). *Clostridium innocuum* I46 and *Flavonifractor plautii* YL31, both well-known

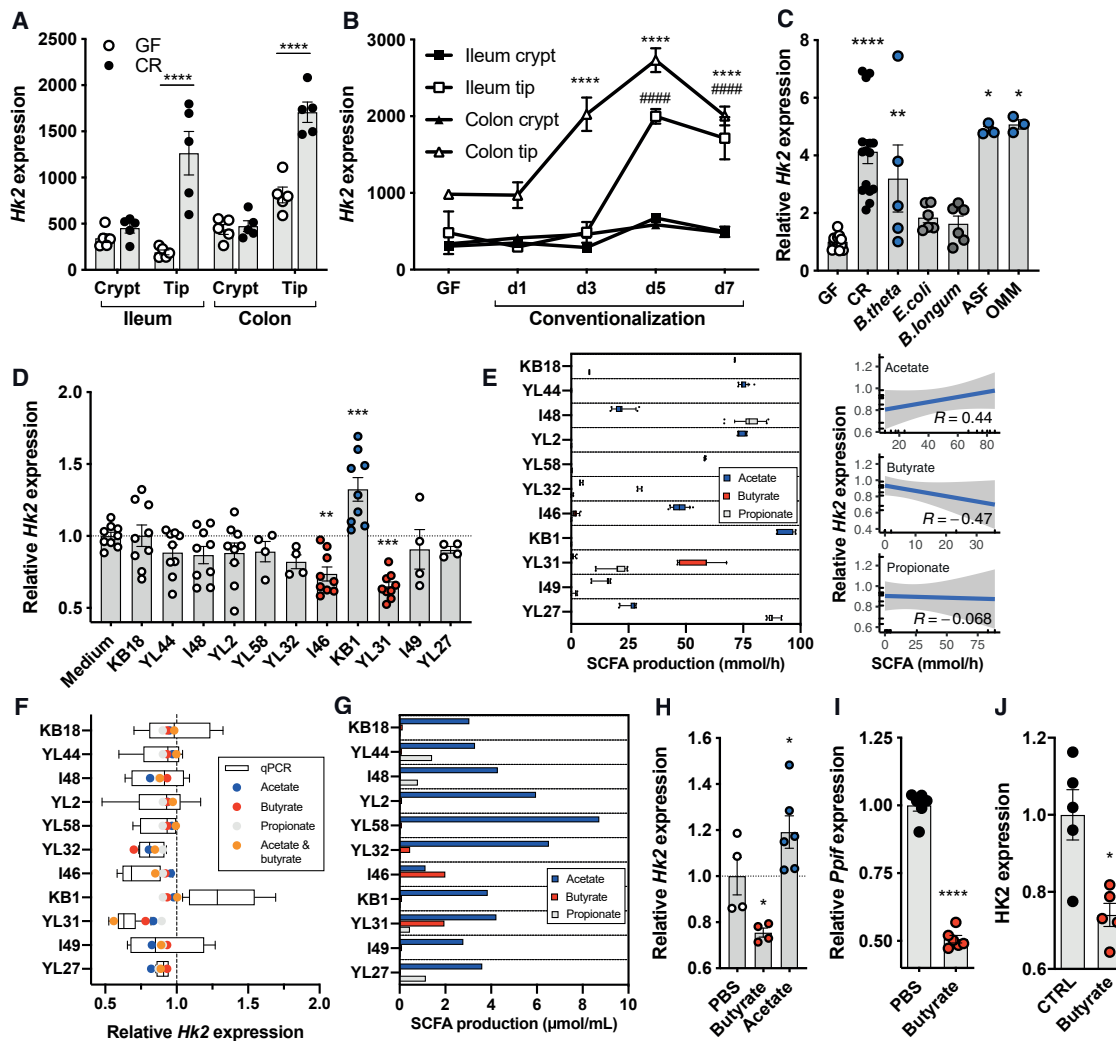


**Figure 3. The microbiota regulates HK2**

(A and B) *Hk2* expression in crypts and tips of ileum and colon of (A) germ-free (GF) and conventionally raised (CR) mice and (B) during colonization of GF mice with a normal microbiota. \*\*\*\* $p < 0.0001$  GF versus CR using moderated t test with FDR correction. #  $p < 0.001$  GF versus d1 or d3 or d5 or d7 using one-way ANOVA. (C) *Hk2* expression in GF mice and those mono-colonized with the single bacteria *Bacteroides thetaiotaomicron* (Gram–), *Escherichia coli* (Gram–) or *Bifidobacterium longum* (Gram+) or the minimal microbiomes ASF (Altered Schaedler Flora) and OMM (Oligo-Mouse-Microbiota). \* $p < 0.05$ , \*\* $p < 0.01$  and \*\*\*\* $p < 0.0001$  versus GF using one-way ANOVA. (D) Relative *Hk2* expression in Caco-2 cells stimulated with sterile-filtered culture supernatants of the OMM species grown *in vitro*. The used strains were: *Acetabacter muris* KB18, *Akkermansia municipiphila* YL44, *Bacteroides caecimuris* I48, *Bifidobacterium animalis* YL2, *Blautia coccoides* YL58, *Enterocloster clostridioforme* YL32, *Clostridium innocuum* I46, *Enterococcus faecalis* KB1, *Flavonifractor plautii* YL31, *Limosilactobacillus reuteri* I49, *Muribaculum intestinale* YL27. \*\* $p < 0.01$  and \*\*\* $p < 0.001$  versus Medium using one-way ANOVA. (E) Metabolic modeling of the production of acetate, butyrate, and propionate by the individual OMM bacteria based on their published genome information and the used *in-vitro* growth conditions, and correlation of metabolite production with *Hk2* expression. R denotes the Pearson correlation coefficient. (F) Prediction of linear models incorporating the acetate, butyrate, and propionate levels to explain the observed changes in *Hk2* expression upon stimulation of Caco-2 cells with the bacterial culture supernatants, shown in (D). (G) SCFA levels quantified in culture supernatants of single OMM bacteria, which were used to stimulate Caco-2 cells, shown in (D). (H) Relative *Hk2* expression in Caco-2 cells stimulated with the microbial metabolites acetate and butyrate (10 mM each for 24 h). \* $p < 0.05$  versus PBS using one-way ANOVA. (I) Relative *Ppif* expression in Caco-2 cells stimulated with butyrate. \*\*\*\* $p < 0.0001$  versus PBS using one-way ANOVA. (J) Feeding WT mice a butyrate-enriched diet reduced HK2 protein expression in colonic epithelium as measured by immunohistochemistry. \* $p < 0.05$  versus CTRL diet using one-way ANOVA. Data are presented as means  $\pm$  SEM.

producers of short-chain fatty acids (SCFA) (Braune and Blaut, 2016), significantly reduced *Hk2* expression (Figure 3D). *Hk2* expression increases along the intestinal tract (Figure S5), coin-

ciding with an increasing bacterial load and reaches its highest expression in the colon (Larsson et al., 2012), the main site of bacterial fermentation (Sommer and Bäckhed, 2016). As other

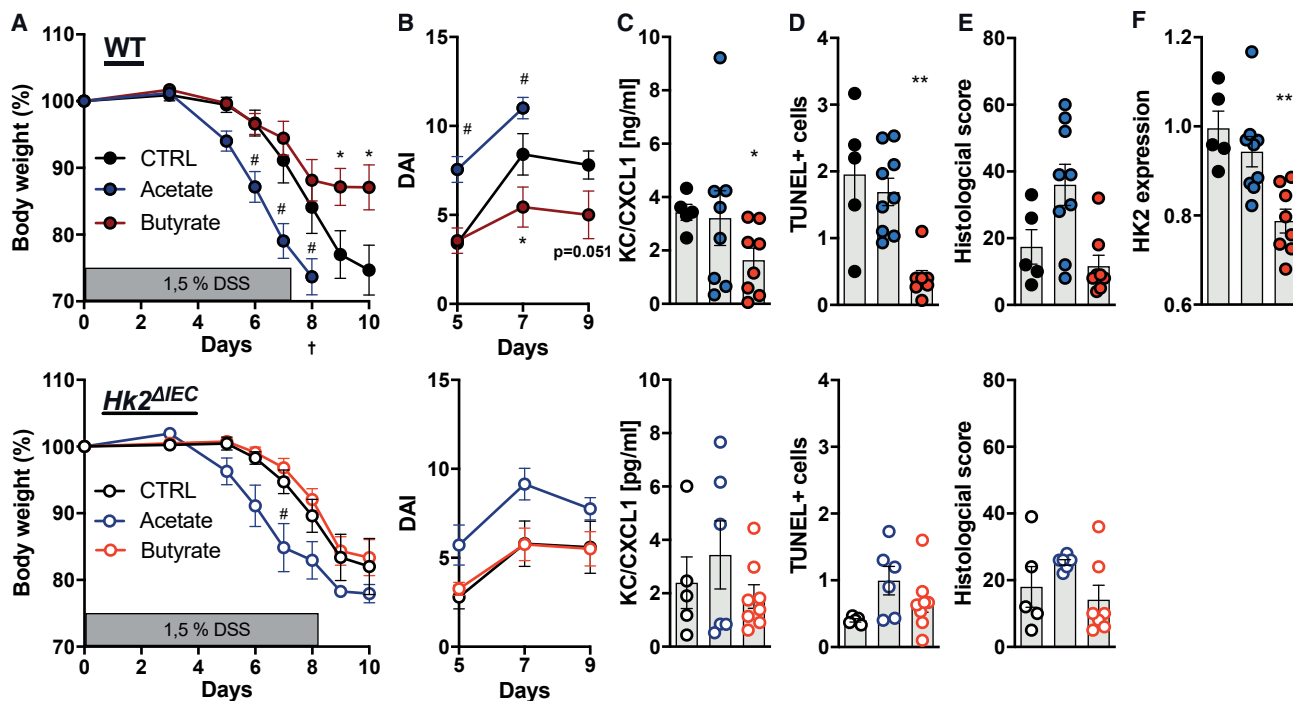


**Figure 4. Dietary supplementation of the microbial metabolite butyrate ameliorates colitis via HK2**

(A–E) WT and *Hk2*<sup>ΔIEC</sup> mice were fed either an acetate-enriched, butyrate-enriched or control diet and were then orally administered DSS to induce colitis. (A) Body weight development, (B) DAI, (C) serum KC/CXCL1 levels, (D) TUNEL-positive cells per colon crypt, (E) histological score of WT (upper panel) and *Hk2*<sup>ΔIEC</sup> (lower panel) mice.

(F) HK2 protein levels in colon epithelium of treated WT mice as per immunohistochemistry. Butyrate repressed HK2 expression. \* / # indicate statistical significance in Butyrate (\*) or Acetate (#) versus CTRL diet using two-way ANOVA in (A and B) and one-way ANOVA in (C–F). Data are presented as means ± SEM.

fatty acids such as palmitic acid can inhibit HK activity (Mogilenko et al., 2019; Weber et al., 1966), we hypothesized that SCFAs could drive the regulation of *Hk2* expression. To test this hypothesis, we generated individual metabolic models predicting the SCFA synthesis potential for each OMM member (Figure 3E). A linear model of the predicted *Hk2* expression based on the butyrate and acetate levels significantly correlated with the experimental *Hk2* expression determined by qPCR (p value = 0.008, Pearson R = 0.75, R<sup>2</sup> = 0.56, AIC = -8.0; Figure 3F; Table S2). The predicted SCFA levels in the OMM culture supernatants were validated by targeted metabolomics (Figure 3G). We next stimulated Caco-2 cells with butyrate and acetate and found that acetate upregulated, whereas butyrate downregulated *Hk2* expression (Figure 3H). We then tested whether stimulation of Caco-2 cells with butyrate also affected *Ppif* expression. Indeed, butyrate also downregulated the expression of *Ppif* (Figure 3I). Together these data suggested that the microbial metabolite butyrate could potentially protect from inflammation via HK2- and PPIF-mediated changes in mitochondrial function and cell death. We therefore tested whether dietary supplementation of butyrate also functions *in vivo* to downregulate HK2 levels. We fed a butyrate-enriched diet to WT mice for 10 days and quantified HK2 levels in colon sections by immunohistochemistry, which demonstrated a clear downregulation of HK2 (Figure 3J).

### The microbial metabolite butyrate ameliorates intestinal inflammation by downregulating HK2

We then set out to test whether the SCFA-dependent modulation of HK2 levels also impacts colitis outcome. Therefore, we supplemented *Hk2*<sup>ΔIEC</sup> mice and their WT littermates with three different diets—a control diet, a butyrate-enriched diet, or an acetate-containing diet—and induced colitis by performing the DSS colitis model as before. Indeed, in WT mice dietary supplementation of butyrate ameliorated colitis, which was evident by a significantly lower weight loss (Figure 4A), lower DAI (Figure 4B), lower serum levels of KC/CXCL1 (Figure 4C), fewer TUNEL-positive epithelial cells (Figure 4D), and a trend toward lower histological inflammation score (Figure 4E). In contrast, acetate supplementation worsened colitis outcome as evident by a significantly increased weight loss (Figure 4A) and a higher DAI (Figure 4B), which even led to premature termination of this experimental group for ethical reasons on day 8. Butyrate supplementation lowered colonic HK2 levels in WT mice (Figure 4F). In *Hk2*<sup>ΔIEC</sup> mice, treatment with butyrate did not impact colitis outcome as measured by weight development, DAI, serum KC/CXCL1 levels, TUNEL-positive epithelial cells, or histological score (Figures 4A–4E and S6). Together these data therefore demonstrate that ablation of HK2 in the intestinal epithelium completely blunted the butyrate-dependent effects on colitis. We then tested whether butyrate treatment modulates mitochondrial function dependent on the HK2 status. To that end

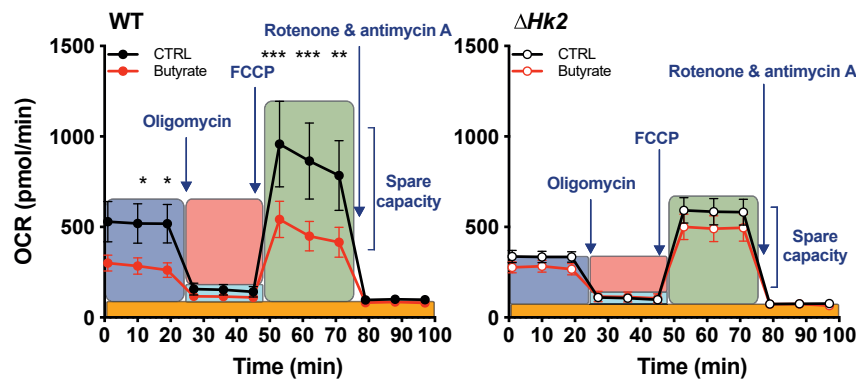


**Figure 5. Butyrate alters mitochondrial function**

Caco-2<sup>WT</sup> and HK2-deficient Caco-2<sup>ΔHk2</sup> cells were treated with 2 mM butyrate for 24 h before measuring the oxygen consumption rate (OCR) as indicator of mitochondrial respiration using the Seahorse XF analyzer. Butyrate reduced mitochondrial respiration in WT but not in HK2-deficient Caco-2 cells. \*p < 0.05, \*\*p < 0.01 and \*\*\*p < 0.001 WT versus  $\Delta Hk2$  using two-way ANOVA. Data are presented as means  $\pm$  SEM.

we pre-treated Caco-2<sup>ΔHk2</sup> and Caco-2<sup>WT</sup> cells with butyrate and measured mitochondrial respiration using Seahorse analysis. Indeed, butyrate lowered the basal and maximal respiration in WT- but not in HK2-deficient Caco-2 cells (Figure 5), which not only matched the reduction of both basal and maximal respiration after loss of HK2 but also correlates with the protective effects of butyrate only in WT but not in *Hk2*<sup>ΔIEC</sup> mice during DSS colitis.

#### HDAC8 mediates the repression of HK2 by butyrate

SCFAs are well-known for their pleiotropic effects on host physiology including intestinal motility, inflammation, and carcinogenesis (Koh et al., 2016). Regarding colitis, acetate was shown to exacerbate (Maslowski et al., 2009), whereas butyrate ameliorates (Chang et al., 2014; Furusawa et al., 2013; Singh et al., 2014) inflammation. Butyrate is produced by the metabolic activity of the colonic microorganisms through fermentation of dietary fiber (Louis et al., 2004). Mechanistically, butyrate is sensed by the G protein-coupled receptors GPR41 (FFAR3) (Brown et al., 2003; De Vadder et al., 2014), GPR43 (FFAR2) (Brown et al., 2003; Le Poul et al., 2003; Nilsson et al., 2003; Sina et al., 2009), and GPR109a (HCAR2) (Macia et al., 2015; Singh et al., 2014), which could trigger a signaling response leading to reduced *Hk2* expression. Combined silencing of these GPRs by siRNAs did not alter repression of *Hk2* expression by butyrate in Caco-2 cells (Figures 6A and 6B), which argues against a prominent role of these GPRs. Alternatively, butyrate also directly acts on histone deacetylases (HDACs) (Koh et al., 2016), which function as epigenetic regulators and thereby could impact on *Hk2* expression. Using either a pan-HDAC inhibitor or class-specific inhibitors, we found that blocking all HDACs or only class I HDACs (HDACs 1, 2, 3, and 8 together) abolished the repression of *Hk2* expression by butyrate (Figure 6C). We then investigated the role of the individual class I HDACs by using single HDAC enzyme-specific inhibitors. Individual inhibition of HDAC1 or HDAC2 or HDAC3 by enzyme-specific inhibitors did not impact the repression of *Hk2* expression by butyrate, whereas an HDAC8 inhibitor abolished the transcriptional repression of *Hk2* by butyrate (Figure 6C), which argues for a specific role of HDAC8 (a class I HDAC) in mediating the butyrate-dependent regulation of *Hk2*.

Taken together, our study revealed a novel regulatory circuit consisting of intestinal epithelial HK2 and the microbial metabolite butyrate. We found that ablation of HK2 protects from colitis by suppression of cell death that was linked to altered mitochon-

drial function, which could be due to PPIF-dependent opening of the MPTP. Moreover, we identified the intestinal microbiota and its metabolite butyrate as potent regulators of HK2, and we demonstrated that the protective effect of dietary butyrate supplementation is dependent on the functional presence of HK2. Previous studies already pointed toward a beneficial function of butyrate-producing bacteria for a healthy intestine and prevention of gut inflammation (Aden et al., 2019; Effenberger et al., 2021; Imhann et al., 2018; Lloyd-Price et al., 2019; Parada Venegas et al., 2019; Sommer et al., 2017), and clinical trials using oral supplementation of germinated barley foods that are fermented into SCFA by the microbiota or rectal enema with butyrate indeed demonstrated beneficial effects in ulcerative colitis patients (Breuer et al., 1991; Mitsuyama et al., 1998). Our findings therefore shed light on the molecular mechanism how butyrate mediates its beneficial effects and may guide the development of more specific therapeutic options by targeting HK2.

#### DISCUSSION

HK2 functions as the main inducible HK isoform. Deleting HK2 in the entire body is embryonically lethal, but heterozygous *Hk2*<sup>+/-</sup> mice with a 50% reduction in *Hk2* are viable and have some minor physiological abnormalities (Fueger et al., 2003; Smeele et al., 2011; Wu et al., 2012) yet do not show an altered glucose metabolism (Heikkinen et al., 1999). We used mice with an IEC-specific conditional knockout of HK2, an isoform of a major glycolytic enzyme, and one could have expected a negative impact on intestinal epithelial or organismal metabolism and viability. However, we observed no differences in cell turnover or cell death under basal conditions (Figures S1L and S1M), nor did we observe any indications of a general energy deficiency in *Hk2*<sup>ΔIEC</sup> mice such as a growth deficiency or lower levels of adipose tissue (Figures S1A and S1E). Moreover, we also did not observe any changes in glycolytic activity using Seahorse analyses in HK2-deficient Caco-2 cells (Figure 2B). Our findings are in line with data from *Hk2*<sup>+/-</sup> mice that also do not exhibit any metabolic impairments (Heikkinen et al., 1999). Alternatively, other HK family members, especially HK1, could potentially compensate for the loss of HK2. Furthermore, intestinal epithelial HK2 may not contribute heavily to blood glucose levels under basal conditions (Figure S1J) but only under stress, e.g., inflammatory challenge. We did, however, observe a mildly improved glucose tolerance in *Hk2*<sup>ΔIEC</sup> mice (Figure S1J). If and how the selective intestinal epithelial ablation of hexokinases can affect intestinal or organismal metabolism will be interesting to address in further studies.

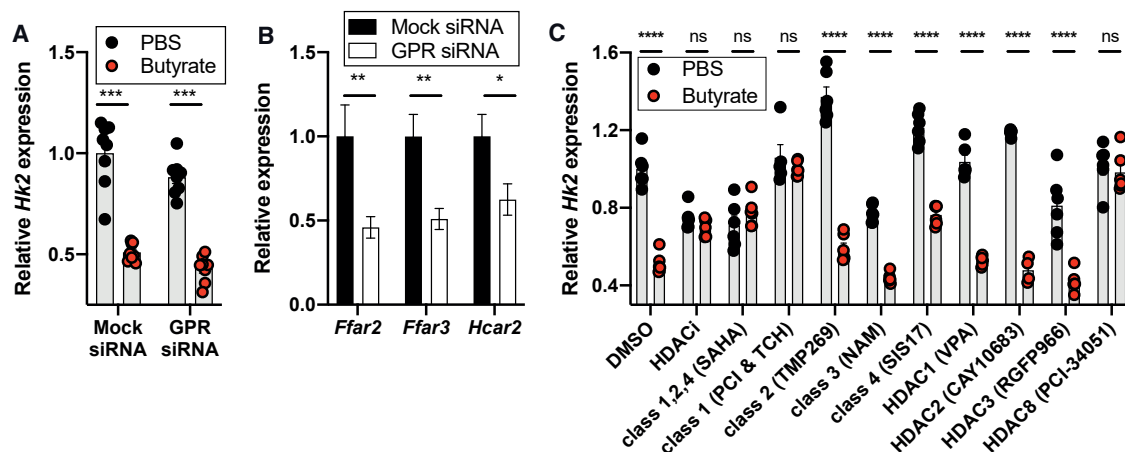


**Figure 6. HDAC8 mediates the repression of *Hk2* expression by butyrate**

(A) Relative *Hk2* expression in Caco-2 cells after transfection with a mix of siRNA targeting the three G protein-coupled receptors (GPR) GPR41 (*Ffar3*), GPR43 (*Ffar2*), and GPR109a (*Hcar2*) and subsequent stimulation with butyrate.

(B) Expression of *Ffar3*, *Ffar2*, and *Hcar2* in Caco-2 cells after transfection with the siRNA targeting these three GPRs to test for successful knockdown.

(C) Relative *Hk2* expression in Caco-2 cells first treated with general or specific HDAC inhibitors and then incubated with butyrate. HDACi refers to a mixture of SAHA (10 $\mu$ M) and NAM (nicotinamide) (10mM) and was used to inhibit all HDAC classes. A mixture of PCI-34051 (10 $\mu$ M) and TC-H106 (5 $\mu$ M) were used to inhibit class I HDACs. TMP269 (5 $\mu$ M), NAM (10mM), and SIS17 (50 $\mu$ M) were used to inhibit class II, III, and IV, respectively. VPA (Valproic acid) (1mM), CAY10682 (10 $\mu$ M), RGFP966 (5 $\mu$ M), and PCI-34051 (10 $\mu$ M) were used to inhibit only HDAC1, HDAC2, HDAC3, and HDAC8, respectively. All expression values were normalized to the mean of DMSO-PBS. Data are presented as means  $\pm$  SEM.

The exact composition of the MPTP is unclear to date (Baines and Gutiérrez-Aguilar, 2018). Earlier studies suggested the adenine nucleotide transporter (ANT), a voltage-dependent anion channel (VDAC), and PPIF to be main components of the MPTP (Baines et al., 2005). However, more recent publications with gain- and loss-of-function experiments questioned a critical involvement of these proteins in the MPTP (Baines and Gutiérrez-Aguilar, 2018). In contrast, inhibition of PPIF has been shown to reduce MPTP opening (Nederlof et al., 2017), thus supporting a key function of PPIF for regulating the MPTP. Here, we did not observe any changes in genes encoding components of VDAC or ANT expression within our RNA sequencing data following the loss of HK2. We, however, found that in HK2-deficient IECs *Ppif* expression was significantly downregulated under inflammatory conditions (Figure 2D). An interaction between PPIF and HK2 has been described previously (Machida et al., 2006; Nederlof et al., 2017). Yet, it is not known to date how these proteins exactly interact with each other. It was suggested that the detachment of HK2 from the outer mitochondrial membrane can induce MPTP-mediated cell death and that mitochondrial binding of HK2 prevents cell death (Machida et al., 2006). This is in line with our findings that HK2-deficient epithelial cells show reduced cell death under inflammatory conditions (Figures 1G and 1H) as well as reduced mitochondrial respiration (Figures 2C and 5). It will be important to assess the molecular composition of the MPTP and how HK2 and/or PPIF potentially contribute to opening of the MPTP in detail in future studies.

We report that *Hk2* expression is induced in CR compared to GF mice (Figures 3A and 3B) but also that the microbial metabolite butyrate repressed *Hk2* expression both *in vitro* and *in vivo* (Figure 3). This may seem contradictory as butyrate is a well-known product of the normal colonic microbiota. CR mice have more than 100-fold higher SCFA levels than GF mice, but

the by far most abundant SCFA is acetate (Høverstad et al., 1985; Krautkramer et al., 2016). Here, we also report that acetate stimulated *Hk2* expression and, thus, we conclude that the high acetate production is most likely a main driver for the observed induction of *Hk2* by the bulk intestinal microbiome in CR mice. Apart from the action of SCFAs, there are also many other physiological differences between GF and CR mice (Sommer and Bäckhed, 2013) that may contribute to the overall microbial induction of *Hk2* expression. As a plethora of bacterial species can produce SCFAs by fermentation of dietary fiber, potentially more bacterial species than those identified here might have the ability to regulate *Hk2* expression. Reductions of the SCFA-producing bacteria have been associated with various inflammatory and metabolic disorders. Therefore, further studies are warranted to elucidate the exact role of bacteria and SCFAs in targeting HK2 in other inflammatory and metabolic diseases.

Finally, we provide first evidence of a novel regulatory circuit between butyrate and *Hk2* in intestinal inflammation. By analyzing expression data from mucosal biopsies of 646 human patients we found that *Hk2* was upregulated irrespective of the type of intestinal inflammation (CD, UC, NIC; Figures 1F–1I). However, *Hk2* has not been described previously as a risk gene for IBD. Therefore, the association of *Hk2* with intestinal inflammation should be explored further in upcoming studies. We have performed all interventional experiments such as butyrate supplementation in animal models and not in humans and therefore emphasize the pre-clinical nature of our study. Earlier studies have already tested oral and rectal butyrate supplementation in IBD patients (Di Sabatino et al., 2007; Di Sabatino et al., 2005; Scheppach et al., 1992), but these studies were low in sample size and also faced technical challenges (no blinded distribution) due to the olfactory properties and side-effects of butyrate. Our findings shed light on the molecular mechanism how butyrate mediates its beneficial effects and

therefore may guide the development of more specific therapeutic options by targeting HK2.

### Limitations of study

Our study was conducted exclusively in male mice. Although we did not observe any obvious gender-specific physiological differences in unchallenged *Hk2*<sup>ΔIEC</sup> mice, there may be a possibility of differential responses under stressed conditions, i.e., inflammatory challenge, due to alternating hormone profiles or inflammatory responses. In humans, published literature points toward gender-related differences in disease incidence and pathologies for chronic intestinal inflammation (Shah et al., 2018).

Furthermore, we used a variety of model systems including animals (mice) and stable intestinal cell lines such as Caco-2 cells. We strongly support the notion that a model system should resemble the *in vivo* situation and potentially a human disease as closely as possible. The used cell line Caco-2 are derived from colon carcinoma cells that may demonstrate different features compared to primary cells. Since no non-carcinogenic human or murine colonic cell line exists, we had to refer to a stable cancer cell line as an *in vitro* model system to perform Seahorse analyses. We therefore cannot rule out a potential bias in the assessment of cell death and metabolism in our model. To the best of our knowledge, there are no primary research publications that use primary cells to perform Seahorse analyses, especially in combination with stimulations over many hours, i.e., butyrate treatment, as these cells are too unstable for a prolonged culture. Experimental solutions seem to be upcoming using intestinal organoids, yet also this approach is extremely challenging due to the 3D structure of organoids that conflicts with the narrow space requirements of the Seahorse technology.

Finally, we only investigated the impact of the deletion of a single HK family member: HK2. At this point, we can't rule out that in the absence of HK2 other HK family members could also contribute to the metabolic or inflammatory functions. Therefore, it will be interesting to investigate this issue in further studies by generating tissue-specific knockout mice with compound deletions of multiple if not all HK genes.

### STAR★METHODS

Detailed methods are provided in the online version of this paper and include the following:

- [KEY RESOURCES TABLE](#)
- [RESOURCE AVAILABILITY](#)
  - Lead contact
  - Material availability
  - Data and code availability
- [EXPERIMENTAL MODEL AND SUBJECT DETAILS](#)
  - Animals
  - Bacteria and *in vitro* culture
  - Culture of Caco-2 cells
  - Culture of intestinal organoids
- [METHOD DETAILS](#)
  - Noggin-conditioned medium
  - R-Spondin-conditioned medium
  - Isolation of primary cells
  - Generation and culture of HK2-deficient Caco-2 cells

- siRNA Transfection
- RNA isolation and qPCR
- RNA sequencing
- Microbiota analysis
- Western blot analyses
- Histology and immunostaining
- Seahorse analysis
- Metabolic modeling of SCFA production by OMM bacteria
- Quantification of SCFAs
- ELISA

### ● [QUANTIFICATION AND STATISTICAL ANALYSIS](#)

### SUPPLEMENTAL INFORMATION

Supplemental information can be found online at <https://doi.org/10.1016/j.cmet.2021.11.004>.

### ACKNOWLEDGMENTS

The authors thank Karina Greve, Dorina Oelsner, Melanie Vollstedt, Maren Reffelmann, Melanie Nebendahl, Sabine Kock, and Stefanie Baumgarten for excellent technical assistance. We also thank Dr. Filipe de Vadder (Lyon University, France) for critical comments that greatly improved the manuscript.

This work was supported by the German Research Foundation (DFG) through the individual grant SO1141/10-1, the Research Training Group "Genes, Environment, and Inflammation" (RTG1743), the Research Unit FOR5042 "miTarget - The Microbiome as a Target in Inflammatory Bowel Diseases" (projects P5, P3, and Z), the Collaborative Research Centre CRC1182 "Origin and Function of Metaorganisms" (projects C2 and A1), the Excellence Clusters EXS2167 "Precision Medicine in Chronic Inflammation," and EXC306 "Inflammation at Interfaces," the Federal Ministry of Education and Research (BMBF) iTREAT SP5 project and via the SH Excellence Chair Program to Philip Rosenstiel. This work was further supported by the DFG CRC1371 "Microbiome Signatures," the European Research Council (EVOGUTHEALTH; grant no. 865615), and the German Center for Infection Research (DZIF).

### AUTHOR CONTRIBUTIONS

F.H., J.H., M.W., L.S., P.R., and F.S. designed research. F.H., J.H., M.W., L.S., N.S., and F.S. managed the conventional mouse colony, monitored the mice, performed animal experiments, and collected samples. M.B., V.T., and F.B. maintained the gnotobiotic mouse facilities, performed the colonizations of GF mice with single bacteria and minimal consortia and provided samples. F.H., J.H., M.W., L.S., A.W., K.S., N.S., K.K., D.P., S.K., D.B., A.F., G.L., S.I., and P.R. conducted the wet lab experiments. F.H., J.H., M.W., L.S., N.M., K.S., N.S., K.K., R.H., S.K., F.B., P.R., and F.S. analyzed and interpreted the data. J.H., N.M., A.W., J.Z., G.M., R.H., and F.S. performed the bioinformatics analyses. F.H., J.H., M.W., L.S., and F.S. prepared the figures. R.A.S., S.K., A.W., B.S., P.S.K., C.K., J.R., and F.B. provided resources. P.R. and F.S. obtained funding. F.H., J.H., M.W., L.S., P.R., and F.S. co-wrote the manuscript with critical input from all authors.

### DECLARATION OF INTERESTS

The authors declare no competing interests.

Received: January 27, 2021

Revised: August 7, 2021

Accepted: November 9, 2021

Published: November 29, 2021

### REFERENCES

Aden, K., Tran, F., Ito, G., Sheibani-Tezerji, R., Lipinski, S., Kuiper, J.W., Tschurtschenthaler, M., Saveljeva, S., Bhattacharyya, J., Häslner, R., et al. (2018). ATG16L1 orchestrates interleukin-22 signaling in the intestinal

- epithelium via cGAS-STING. *J. Exp. Med.* 215, 2868–2886. <https://doi.org/10.1084/jem.20171029>.
- Aden, K., Rehman, A., Waschina, S., Pan, W.H., Walker, A., Lucio, M., Nunez, A.M., Bharti, R., Zimmerman, J., Bethge, J., et al. (2019). Metabolic Functions of Gut Microbes Associate With Efficacy of Tumor Necrosis Factor Antagonists in Patients With Inflammatory Bowel Diseases. *Gastroenterology* 157, 1279–1292.e11. <https://doi.org/10.1053/j.gastro.2019.07.025>.
- Baines, C.P., and Gutiérrez-Aguilar, M. (2018). The still uncertain identity of the channel-forming unit(s) of the mitochondrial permeability transition pore. *Cell Calcium* 73, 121–130. <https://doi.org/10.1016/j.ceca.2018.05.003>.
- Baines, C.P., Kaiser, R.A., Purcell, N.H., Blair, N.S., Osinska, H., Hambleton, M.A., Brunskill, E.W., Sayen, M.R., Gottlieb, R.A., Dorn, G.W., et al. (2005). Loss of cyclophilin D reveals a critical role for mitochondrial permeability transition in cell death. *Nature* 434, 658–662. <https://doi.org/10.1038/nature03434>.
- Basso, E., Fante, L., Fowlkes, J., Petronilli, V., Forte, M.A., and Bernardi, P. (2005). Properties of the permeability transition pore in mitochondria devoid of Cyclophilin D. *J. Biol. Chem.* 280, 18558–18561. <https://doi.org/10.1074/jbc.C500089200>.
- Beutner, G., Alanzalon, R.E., and Porter, G.A., Jr. (2017). Cyclophilin D regulates the dynamic assembly of mitochondrial ATP synthase into synthasomes. *Sci. Rep.* 7, 14488. <https://doi.org/10.1038/s41598-017-14795-x>.
- Bolsega, S., Basic, M., Smoczek, A., Buettner, M., Eberl, C., Ahrens, D., Odum, K.A., Stecher, B., and Bleich, A. (2019). Composition of the Intestinal Microbiota Determines the Outcome of Virus-Triggered Colitis in Mice. *Front. Immunol.* 10, 1708. <https://doi.org/10.3389/fimmu.2019.01708>.
- Bonora, M., and Pinton, P. (2014). The mitochondrial permeability transition pore and cancer: molecular mechanisms involved in cell death. *Front. Oncol.* 4, 302. <https://doi.org/10.3389/fonc.2014.00302>.
- Braune, A., and Blaut, M. (2016). Bacterial species involved in the conversion of dietary flavonoids in the human gut. *Gut Microbes* 7, 216–234. <https://doi.org/10.1080/19490976.2016.1158395>.
- Breuer, R.I., Buto, S.K., Christ, M.L., Bean, J., Vernia, P., Paoluzi, P., Di Paolo, M.C., and Caprilli, R. (1991). Rectal irrigation with short-chain fatty acids for distal ulcerative colitis. Preliminary report. *Dig. Dis. Sci.* 36, 185–187.
- Briston, T., Roberts, M., Lewis, S., Powney, B., M Staddon, J., Szabadkai, G., and Duchon, M.R. (2017). Mitochondrial permeability transition pore: sensitivity to opening and mechanistic dependence on substrate availability. *Sci. Rep.* 7, 10492. <https://doi.org/10.1038/s41598-017-10673-8>.
- Brown, A.J., Goldsworthy, S.M., Barnes, A.A., Eilert, M.M., Tcheang, L., Daniels, D., Muir, A.I., Wigglesworth, M.J., Kinghorn, I., Fraser, N.J., et al. (2003). The Orphan G protein-coupled receptors GPR41 and GPR43 are activated by propionate and other short chain carboxylic acids. *J. Biol. Chem.* 278, 11312–11319. <https://doi.org/10.1074/jbc.M211609200>.
- Brugiroux, S., Beutler, M., Pfann, C., Garzetti, D., Ruscheweyh, H.J., Ring, D., Diehl, M., Herp, S., Lötscher, Y., Hussain, S., et al. (2016). Genome-guided design of a defined mouse microbiota that confers colonization resistance against *Salmonella enterica* serovar Typhimurium. *Nat. Microbiol.* 2, 16215. <https://doi.org/10.1038/nmicrobiol.2016.215>.
- Caporaso, J.G., Bittinger, K., Bushman, F.D., DeSantis, T.Z., Andersen, G.L., and Knight, R. (2010a). PyNAST: a flexible tool for aligning sequences to a template alignment. *Bioinformatics* 26, 266–267. <https://doi.org/10.1093/bioinformatics/btp636>.
- Caporaso, J.G., Kuczynski, J., Stombaugh, J., Bittinger, K., Bushman, F.D., Costello, E.K., Fierer, N., Peña, A.G., Goodrich, J.K., Gordon, J.I., et al. (2010b). QIIME allows analysis of high-throughput community sequencing data. *Nat. Methods* 7, 335–336. <https://doi.org/10.1038/nmeth.f.303>.
- Chang, P.V., Hao, L., Offermanns, S., and Medzhitov, R. (2014). The microbial metabolite butyrate regulates intestinal macrophage function via histone deacetylase inhibition. *Proc. Natl. Acad. Sci. USA* 111, 2247–2252. <https://doi.org/10.1073/pnas.1322269111>.
- De Vadder, F., Kovatcheva-Datchary, P., Goncalves, D., Vinera, J., Zitoun, C., Duchamp, A., Bäckhed, F., and Mithieux, G. (2014). Microbiota-generated metabolites promote metabolic benefits via gut-brain neural circuits. *Cell* 156, 84–96. <https://doi.org/10.1016/j.cell.2013.12.016>.
- DeSantis, T.Z., Hugenholtz, P., Larsen, N., Rojas, M., Brodie, E.L., Keller, K., Huber, T., Dalevi, D., Hu, P., and Andersen, G.L. (2006). Greengenes, a chimera-checked 16S rRNA gene database and workbench compatible with ARB. *Appl. Environ. Microbiol.* 72, 5069–5072. <https://doi.org/10.1128/AEM.03006-05>.
- Desouki, A.A., Jarre, F., Gelius-Dietrich, G., and Lercher, M.J. (2015). CycleFreeFlux: efficient removal of thermodynamically infeasible loops from flux distributions. *Bioinformatics* 31, 2159–2165. <https://doi.org/10.1093/bioinformatics/btv096>.
- Dewhirst, F.E., Chien, C.C., Paster, B.J., Ericson, R.L., Orcutt, R.P., Schauer, D.B., and Fox, J.G. (1999). Phylogeny of the defined murine microbiota: altered Schaedler flora. *Appl. Environ. Microbiol.* 65, 3287–3292.
- Di Sabatino, A., Morera, R., Ciccocioppo, R., Cazzola, P., Gotti, S., Tinazzi, F.P., Tinazzi, S., and Corazza, G.R. (2005). Oral butyrate for mildly to moderately active Crohn's disease. *Aliment. Pharmacol. Ther.* 22, 789–794. <https://doi.org/10.1111/j.1365-2036.2005.02639.x>.
- Di Sabatino, A., Cazzola, P., Ciccocioppo, R., Morera, R., Biancheri, P., Rovedatti, L., Cantoro, L., Vanoli, A., Tinazzi, F.P., Tinazzi, S., and Corazza, G.R. (2007). Efficacy of butyrate in the treatment of mild to moderate Crohn's disease. *Digestive and Liver Disease Supplements* 1, 31–35. [https://doi.org/10.1016/S1594-5804\(08\)60009-1](https://doi.org/10.1016/S1594-5804(08)60009-1).
- Edgar, R.C. (2010). Search and clustering orders of magnitude faster than BLAST. *Bioinformatics* 26, 2460–2461. <https://doi.org/10.1093/bioinformatics/btq461>.
- Effenberger, M., Reider, S., Waschina, S., Bronowski, C., Enrich, B., Adolph, T.E., Koch, R., Moschen, A.R., Rosenstiel, P., Aden, K., and Tilg, H. (2021). Microbial butyrate synthesis indicates therapeutic efficacy of azathioprine in IBD patients. *J. Crohn's Colitis* 15, 88–98. <https://doi.org/10.1093/ecco-jcc/jjaa152>.
- Egorin, M.J., Yuan, Z.M., Sentz, D.L., Plaisance, K., and Eiseman, J.L. (1999). Plasma pharmacokinetics of butyrate after intravenous administration of sodium butyrate or oral administration of tributyrin or sodium butyrate to mice and rats. *Cancer Chemother. Pharmacol.* 43, 445–453. <https://doi.org/10.1007/s002800050922>.
- Everts, B., Amiel, E., Huang, S.C.-C., Smith, A.M., Chang, C.-H., Lam, W.Y., Redmann, V., Freitas, T.C., Blagih, J., van der Windt, G.J.W., et al. (2014). TLR-driven early glycolytic reprogramming via the kinases TBK1-IKKε supports the anabolic demands of dendritic cell activation. *Nat. Immunol.* 15, 323–332. <https://doi.org/10.1038/ni.2833>.
- Fueger, P.T., Heikkinen, S., Bracy, D.P., Malabanan, C.M., Pencek, R.R., Laakso, M., and Wasserman, D.H. (2003). Hexokinase II partial knockout impairs exercise-stimulated glucose uptake in oxidative muscles of mice. *Am. J. Physiol. Endocrinol. Metab.* 285, E958–E963. <https://doi.org/10.1152/ajpendo.00190.2003>.
- Fulde, M., Sommer, F., Chassaing, B., van Vorst, K., Dupont, A., Hensel, M., Basic, M., Klopffleisch, R., Rosenstiel, P., Bleich, A., et al. (2018). Neonatal selection by Toll-like receptor 5 influences long-term gut microbiota composition. *Nature* 560, 489–493. <https://doi.org/10.1038/s41586-018-0395-5>.
- Furusawa, Y., Obata, Y., Fukuda, S., Endo, T.A., Nakato, G., Takahashi, D., Nakanishi, Y., Uetake, C., Kato, K., Kato, T., et al. (2013). Commensal microbe-derived butyrate induces the differentiation of colonic regulatory T cells. *Nature* 504, 446–450. <https://doi.org/10.1038/nature12721>.
- Goodman, A.L., McNulty, N.P., Zhao, Y., Leip, D., Mitra, R.D., Lozupone, C.A., Knight, R., and Gordon, J.I. (2009). Identifying genetic determinants needed to establish a human gut symbiont in its habitat. *Cell Host Microbe* 6, 279–289. <https://doi.org/10.1016/j.chom.2009.08.003>.
- Gupta, J., and Nebreda, A.R. (2014). Analysis of Intestinal Permeability in Mice. *Biol.-protocol* 4, e1289. <https://doi.org/10.21769/BioProtoc.1289>.
- Haas, B.J., Gevers, D., Earl, A.M., Feldgarden, M., Ward, D.V., Giannoukos, G., Ciulla, D., Tabbaa, D., Highlander, S.K., Sodergren, E., et al.; Human Microbiome Consortium (2011). Chimeric 16S rRNA sequence formation and detection in Sanger and 454-pyrosequenced PCR amplicons. *Genome Res.* 21, 494–504. <https://doi.org/10.1101/gr.112730.110>.

- Haberman, Y., Tickle, T.L., Dexheimer, P.J., Kim, M.O., Tang, D., Karns, R., Baldassano, R.N., Noe, J.D., Rosh, J., Markowitz, J., et al. (2014). Pediatric Crohn disease patients exhibit specific ileal transcriptome and microbiome signature. *J. Clin. Invest.* *124*, 3617–3633. <https://doi.org/10.1172/JCI75436>.
- Häsler, R., Sheibani-Tezerji, R., Sinha, A., Barann, M., Rehman, A., Esser, D., Aden, K., Knecht, C., Brandt, B., Nikolaus, S., et al. (2017). Uncoupling of mucosal gene regulation, mRNA splicing and adherent microbiota signatures in inflammatory bowel disease. *Gut* *66*, 2087–2097. <https://doi.org/10.1136/gutjnl-2016-311651>.
- Heikkinen, S., Pietilä, M., Halmekytö, M., Suppola, S., Pirinen, E., Deeb, S.S., Jänne, J., and Laakso, M. (1999). Hexokinase II-deficient mice. Prenatal death of homozygotes without disturbances in glucose tolerance in heterozygotes. *J. Biol. Chem.* *274*, 22517–22523. <https://doi.org/10.1074/jbc.274.32.22517>.
- Høverstad, T., Midtvedt, T., and Bøhmer, T. (1985). Short-chain fatty acids in intestinal content of germfree mice monocontaminated with *Escherichia coli* or *Clostridium difficile*. *Scand. J. Gastroenterol.* *20*, 373–380. <https://doi.org/10.3109/00365528509091667>.
- Imhann, F., Vich Vila, A., Bonder, M.J., Fu, J., Gevers, D., Visschedijk, M.C., Spekhorst, L.M., Alberts, R., Franke, L., van Dullemen, H.M., et al. (2018). Interplay of host genetics and gut microbiota underlying the onset and clinical presentation of inflammatory bowel disease. *Gut* *67*, 108–119. <https://doi.org/10.1136/gutjnl-2016-312135>.
- Karow, M., and Georgopoulos, C. (1992). Isolation and characterization of the *Escherichia coli* msbB gene, a multicopy suppressor of null mutations in the high-temperature requirement gene htrB. *J. Bacteriol.* *174*, 702–710. <https://doi.org/10.1128/jb.174.3.702-710.1992>.
- Koh, A., De Vadder, F., Kovatcheva-Datchary, P., and Bäckhed, F. (2016). From Dietary Fiber to Host Physiology: Short-Chain Fatty Acids as Key Bacterial Metabolites. *Cell* *165*, 1332–1345. <https://doi.org/10.1016/j.cell.2016.05.041>.
- Krautkramer, K.A., Kreznar, J.H., Romano, K.A., Vivas, E.I., Barrett-Wilt, G.A., Rabaglia, M.E., Keller, M.P., Attie, A.D., Rey, F.E., and Denu, J.M. (2016). Diet-Microbiota Interactions Mediate Global Epigenetic Programming in Multiple Host Tissues. *Mol. Cell* *64*, 982–992. <https://doi.org/10.1016/j.molcel.2016.10.025>.
- Larsson, E., Tremaroli, V., Lee, Y.S., Koren, O., Nookaew, I., Fricker, A., Nielsen, J., Ley, R.E., and Bäckhed, F. (2012). Analysis of gut microbial regulation of host gene expression along the length of the gut and regulation of gut microbial ecology through MyD88. *Gut* *61*, 1124–1131. <https://doi.org/10.1136/gutjnl-2011-301104>.
- Le Poul, E., Loison, C., Struyf, S., Springael, J.Y., Lannoy, V., Decobecq, M.E., Brezillon, S., Dupriez, V., Vassart, G., Van Damme, J., et al. (2003). Functional characterization of human receptors for short chain fatty acids and their role in polymorphonuclear cell activation. *J. Biol. Chem.* *278*, 25481–25489. <https://doi.org/10.1074/jbc.M301403200>.
- Lewis, N.E., Hixson, K.K., Conrad, T.M., Lerman, J.A., Charusanti, P., Polpitiya, A.D., Adkins, J.N., Schramm, G., Purvine, S.O., Lopez-Ferrer, D., et al. (2010). Omic data from evolved *E. coli* are consistent with computed optimal growth from genome-scale models. *Mol. Syst. Biol.* *6*, 390. <https://doi.org/10.1038/msb.2010.47>.
- Li, B., Chauvin, C., De Paulis, D., De Oliveira, F., Gharib, A., Vial, G., Lablanche, S., Leverage, X., Bernardi, P., Ovize, M., and Fontaine, E. (2012). Inhibition of complex I regulates the mitochondrial permeability transition through a phosphate-sensitive inhibitory site masked by cyclophilin D. *Biochim. Biophys. Acta* *1817*, 1628–1634. <https://doi.org/10.1016/j.bbabo.2012.05.011>.
- Li, Y., Jia, A., Wang, Y., Dong, L., Wang, Y., He, Y., Wang, S., Cao, Y., Yang, H., Bi, Y., and Liu, G. (2019). Immune effects of glycolysis or oxidative phosphorylation metabolic pathway in protecting against bacterial infection. *J. Cell. Physiol.* *234*, 20298–20309. <https://doi.org/10.1002/jcp.28630>.
- Liebesch, G., Ecker, J., Roth, S., Schweizer, S., Öttl, V., Schött, H.F., Yoon, H., Haller, D., Holler, E., Burkhardt, R., and Matysik, S. (2019). Quantification of Fecal Short Chain Fatty Acids by Liquid Chromatography Tandem Mass Spectrometry—Investigation of Pre-Analytic Stability. *Biomolecules* *9*, E121. <https://doi.org/10.3390/biom9040121>.
- Lloyd-Price, J., Arze, C., Ananthakrishnan, A.N., Schirmer, M., Avila-Pacheco, J., Poon, T.W., Andrews, E., Ajami, N.J., Bonham, K.S., Brislaw, C.J., et al.; IBDMDB Investigators (2019). Multi-omics of the gut microbial ecosystem in inflammatory bowel diseases. *Nature* *569*, 655–662. <https://doi.org/10.1038/s41586-019-1237-9>.
- Louis, P., Duncan, S.H., McCrae, S.I., Millar, J., Jackson, M.S., and Flint, H.J. (2004). Restricted distribution of the butyrate kinase pathway among butyrate-producing bacteria from the human colon. *J. Bacteriol.* *186*, 2099–2106. <https://doi.org/10.1128/jb.186.7.2099-2106.2004>.
- Love, M.I., Huber, W., and Anders, S. (2014). Moderated estimation of fold change and dispersion for RNA-seq data with DESeq2. *Genome Biol.* *15*, 550. <https://doi.org/10.1186/PREACCEPT-8897612761307401>.
- Machida, K., Ohta, Y., and Osada, H. (2006). Suppression of apoptosis by cyclophilin D via stabilization of hexokinase II mitochondrial binding in cancer cells. *J. Biol. Chem.* *281*, 14314–14320. <https://doi.org/10.1074/jbc.M513297200>.
- Macia, L., Tan, J., Vieira, A.T., Leach, K., Stanley, D., Luong, S., Maruya, M., Ian McKenzie, C., Hijikata, A., Wong, C., et al. (2015). Metabolite-sensing receptors GPR43 and GPR109A facilitate dietary fibre-induced gut homeostasis through regulation of the inflammasome. *Nat. Commun.* *6*, 6734. <https://doi.org/10.1038/ncomms7734>.
- Marigorta, U.M., Denson, L.A., Hyams, J.S., Mondal, K., Prince, J., Walters, T.D., Griffiths, A., Noe, J.D., Crandall, W.V., Rosh, J.R., et al. (2017). Transcriptional risk scores link GWAS to eQTLs and predict complications in Crohn's disease. *Nat. Genet.* *49*, 1517–1521. <https://doi.org/10.1038/ng.3936>.
- Maslowski, K.M., Vieira, A.T., Ng, A., Kranich, J., Sierro, F., Yu, D., Schilter, H.C., Rolph, M.S., Mackay, F., Artis, D., et al. (2009). Regulation of inflammatory responses by gut microbiota and chemoattractant receptor GPR43. *Nature* *461*, 1282–1286. <https://doi.org/10.1038/nature08530>.
- Mitsuyama, K., Saiki, T., Kanauchi, O., Iwanaga, T., Tomiyasu, N., Nishiyama, T., Tateishi, H., Shirachi, A., Ide, M., Suzuki, A., et al. (1998). Treatment of ulcerative colitis with germinated barley foodstuff feeding: a pilot study. *Aliment. Pharmacol. Ther.* *12*, 1225–1230.
- Miyoshi, H., and Stappenbeck, T.S. (2013). In vitro expansion and genetic modification of gastrointestinal stem cells in spheroid culture. *Nat. Protoc.* *8*, 2471–2482. <https://doi.org/10.1038/nprot.2013.153>.
- Moglienko, D.A., Haas, J.T., L'Homme, L., Fleury, S., Quemener, S., Levavasseur, M., Becquart, C., Wartelle, J., Bogomolova, A., Pineau, L., et al. (2019). Metabolic and Innate Immune Cues Merge into a Specific Inflammatory Response via the UPR. *Cell* *177*, 1201–1216.e19. <https://doi.org/10.1016/j.cell.2019.03.018>.
- Nakagawa, T., Shimizu, S., Watanabe, T., Yamaguchi, O., Otsu, K., Yamagata, H., Inohara, H., Kubo, T., and Tsujimoto, Y. (2005). Cyclophilin D-dependent mitochondrial permeability transition regulates some necrotic but not apoptotic cell death. *Nature* *434*, 652–658. <https://doi.org/10.1038/nature03417>.
- Nederlof, R., van den Elshout, M.A.M., Koeman, A., Uthman, L., Koning, I., Eerbeek, O., Weber, N.C., Hollmann, M.W., and Zuurbier, C.J. (2017). Cyclophilin D ablation is associated with increased end-ischemic mitochondrial hexokinase activity. *Sci. Rep.* *7*, 12749. <https://doi.org/10.1038/s41598-017-13096-7>.
- Nilsson, N.E., Kotarsky, K., Owman, C., and Olde, B. (2003). Identification of a free fatty acid receptor, FFA2R, expressed on leukocytes and activated by short-chain fatty acids. *Biochem. Biophys. Res. Commun.* *303*, 1047–1052. [https://doi.org/10.1016/s0006-291x\(03\)00488-1](https://doi.org/10.1016/s0006-291x(03)00488-1).
- Pan, W.H., Sommer, F., Falk-Paulsen, M., Ulas, T., Best, P., Fazio, A., Kachroo, P., Luzius, A., Jentzsch, M., Rehman, A., et al. (2018). Exposure to the gut microbiota drives distinct methylome and transcriptome changes in intestinal epithelial cells during postnatal development. *Genome Med.* *10*, 27. <https://doi.org/10.1186/s13073-018-0534-5>.
- Parada Venegas, D., De la Fuente, M.K., Landskron, G., González, M.J., Quera, R., Dijkstra, G., Harmsen, H.J.M., Faber, K.N., and Héros, M.A. (2019). Short Chain Fatty Acids (SCFAs)-Mediated Gut Epithelial and Immune Regulation and Its Relevance for Inflammatory Bowel Diseases. *Front. Immunol.* *10*, 277. <https://doi.org/10.3389/fimmu.2019.00277>.
- Perrin-Cocon, L., Aublin-Gex, A., Diaz, O., Ramière, C., Peri, F., André, P., and Lotteau, V. (2018). Toll-like Receptor 4-Induced Glycolytic Burst in Human

- Monocyte-Derived Dendritic Cells Results from p38-Dependent Stabilization of HIF-1 $\alpha$  and Increased Hexokinase II Expression. *J. Immunol.* 201, 1510–1521. <https://doi.org/10.4049/jimmunol.1701522>.
- Price, M.N., Dehal, P.S., and Arkin, A.P. (2010). FastTree 2—approximately maximum-likelihood trees for large alignments. *PLoS ONE* 5, e9490. <https://doi.org/10.1371/journal.pone.0009490>.
- Quraishi, M.N., Acharjee, A., Beggs, A.D., Horniblow, R., Tselepis, C., Gkoutos, G., Ghosh, S., Rossiter, A.E., Loman, N., van Schaik, W., et al. (2020). A Pilot Integrative Analysis of Colonic Gene Expression, Gut Microbiota, and Immune Infiltration in Primary Sclerosing Cholangitis-Inflammatory Bowel Disease: Association of Disease With Bile Acid Pathways. *J. Crohn's Colitis* 14, 935–947. <https://doi.org/10.1093/ecco-jcc/jjaa021>.
- Sato, T., Vries, R.G., Snippert, H.J., van de Wetering, M., Barker, N., Stange, D.E., van Es, J.H., Abo, A., Kujala, P., Peters, P.J., and Clevers, H. (2009). Single Lgr5 stem cells build crypt-villus structures in vitro without a mesenchymal niche. *Nature* 459, 262–265. <https://doi.org/10.1038/nature07935>.
- Sato, T., Stange, D.E., Ferrante, M., Vries, R.G., Van Es, J.H., Van den Brink, S., Van Houdt, W.J., Pronk, A., Van Gorp, J., Siersema, P.D., and Clevers, H. (2011). Long-term expansion of epithelial organoids from human colon, adenoma, adenocarcinoma, and Barrett's epithelium. *Gastroenterology* 141, 1762–1772. <https://doi.org/10.1053/j.gastro.2011.07.050>.
- Schaedler, R.W., Dubos, R., and Costello, R. (1965). The Development of the Bacterial Flora in the Gastrointestinal Tract of Mice. *J. Exp. Med.* 122, 59–66.
- Scheppach, W., Sommer, H., Kirchner, T., Paganelli, G.-M., Bartram, P., Christl, S., Richter, F., Dusel, G., and Kasper, H. (1992). Effect of butyrate enemas on the colonic mucosa in distal ulcerative colitis. *Gastroenterology* 103, 51–56. [https://doi.org/10.1016/0016-5085\(92\)91094-K](https://doi.org/10.1016/0016-5085(92)91094-K).
- Schinzler, A.C., Takeuchi, O., Huang, Z., Fisher, J.K., Zhou, Z., Rubens, J., Hetz, C., Danial, N.N., Moskowitz, M.A., and Korsmeyer, S.J. (2005). Cyclophilin D is a component of mitochondrial permeability transition and mediates neuronal cell death after focal cerebral ischemia. *Proc. Natl. Acad. Sci. USA* 102, 12005–12010. <https://doi.org/10.1073/pnas.0505294102>.
- Shah, S.C., Khalili, H., Gower-Rousseau, C., Olen, O., Benchimol, E.I., Lyng, E., Nielsen, K.R., Brassard, P., Vutcovici, M., Bitton, A., et al. (2018). Sex-Based Differences in Incidence of Inflammatory Bowel Diseases—Pooled Analysis of Population-Based Studies From Western Countries. *Gastroenterology* 155, 1079–1089.e3. <https://doi.org/10.1053/j.gastro.2018.06.043>.
- Siegmund, B., Lehr, H.A., Fantuzzi, G., and Dinarello, C.A. (2001). IL-1 beta-converting enzyme (caspase-1) in intestinal inflammation. *Proc. Natl. Acad. Sci. USA* 98, 13249–13254. <https://doi.org/10.1073/pnas.231473998>.
- Sina, C., Gavrilova, O., Förster, M., Till, A., Derer, S., Hildebrand, F., Raabe, B., Chalaris, A., Scheller, J., Rehmann, A., et al. (2009). G protein-coupled receptor 43 is essential for neutrophil recruitment during intestinal inflammation. *J. Immunol.* 183, 7514–7522. <https://doi.org/10.4049/jimmunol.0900063>.
- Singh, N., Gurav, A., Sivaprakasam, S., Brady, E., Padia, R., Shi, H., Thangaraju, M., Prasad, P.D., Manicassamy, S., Munn, D.H., et al. (2014). Activation of Gpr109a, receptor for niacin and the commensal metabolite butyrate, suppresses colonic inflammation and carcinogenesis. *Immunity* 40, 128–139. <https://doi.org/10.1016/j.immuni.2013.12.007>.
- Smeele, K.M., Southworth, R., Wu, R., Xie, C., Nederlof, R., Warley, A., Nelson, J.K., van Horssen, P., van den Wijngaard, J.P., Heikkinen, S., et al. (2011). Disruption of hexokinase II-mitochondrial binding blocks ischemic preconditioning and causes rapid cardiac necrosis. *Circ. Res.* 108, 1165–1169. <https://doi.org/10.1161/CIRCRESAHA.111.244962>.
- Sommer, F., and Bäckhed, F. (2013). The gut microbiota—masters of host development and physiology. *Nat. Rev. Microbiol.* 11, 227–238. <https://doi.org/10.1038/nrmicro2974>.
- Sommer, F., and Bäckhed, F. (2016). Know your neighbor: Microbiota and host epithelial cells interact locally to control intestinal function and physiology. *BioEssays* 38, 455–464. <https://doi.org/10.1002/bies.201500151>.
- Sommer, F., Adam, N., Johansson, M.E.V., Xia, L., Hansson, G.C., and Bäckhed, F. (2014). Altered mucus glycosylation in core 1 O-glycan-deficient mice affects microbiota composition and intestinal architecture. *PLoS ONE* 9, e85254.
- Sommer, F., Nookaew, I., Sommer, N., Fogelstrand, P., and Bäckhed, F. (2015). Site-specific programming of the host epithelial transcriptome by the gut microbiota. *Genome Biol.* 16, 62. <https://doi.org/10.1186/s13059-015-0614-4>.
- Sommer, F., Ståhlman, M., Ilkayeva, O., Arnemo, J.M., Kindberg, J., Josefsson, J., Newgard, C.B., Fröbert, O., and Bäckhed, F. (2016). The Gut Microbiota Modulates Energy Metabolism in the Hibernating Brown Bear *Ursus arctos*. *Cell Rep.* 14, 1655–1661.
- Sommer, F., Rühlemann, M.C., Bang, C., Höppner, M., Rehman, A., Kaleta, C., Schmitt-Kopplin, P., Dempfle, A., Weidinger, S., Ellinghaus, E., et al. (2017). Microbiomarkers in inflammatory bowel diseases: caveats come with caviar. *Gut* 66, 1734–1738. <https://doi.org/10.1136/gutjnl-2016-313678>.
- Straus, D.S. (2013). TNF $\alpha$  and IL-17 cooperatively stimulate glucose metabolism and growth factor production in human colorectal cancer cells. *Mol. Cancer* 12, 78.
- Tabula Muris Consortium; Overall coordination; Logistical coordination; Organ collection and processing; Library preparation and sequencing; Computational data analysis; Cell type annotation; Writing group; Supplemental text writing group; Principal investigators (2018). Single-cell transcriptomics of 20 mouse organs creates a Tabula Muris. *Nature* 562, 367–372. <https://doi.org/10.1038/s41586-018-0590-4>.
- Taman, H., Fenton, C.G., Hensel, I.V., Anderssen, E., Florholmen, J., and Paulssen, R.H. (2018). Genome-wide DNA Methylation in Treatment-naïve Ulcerative Colitis. *J. Crohn's Colitis* 12, 1338–1347. <https://doi.org/10.1093/ecco-jcc/jjy117>.
- Thaiss, C.A., Levy, M., Grosheva, I., Zheng, D., Soffer, E., Blacher, E., Braverman, S., Tengeler, A.C., Barak, O., Elazar, M., et al. (2018). Hyperglycemia drives intestinal barrier dysfunction and risk for enteric infection. *Science* 359, 1376–1383.
- Weber, G., Convery, H.J., Lea, M.A., and Stamm, N.B. (1966). Feedback inhibition of key glycolytic enzymes in liver: action of free fatty acids. *Science* 154, 1357–1360.
- Weiser, M., Simon, J.M., Kochar, B., Tovar, A., Israel, J.W., Robinson, A., Gipson, G.R., Schaner, M.S., Herfarth, H.H., Sartor, R.B., et al. (2018). Molecular classification of Crohn's disease reveals two clinically relevant subtypes. *Gut* 67, 36–42. <https://doi.org/10.1136/gutjnl-2016-312518>.
- Weiss, J.N., Korge, P., Honda, H.M., and Ping, P. (2003). Role of the mitochondrial permeability transition in myocardial disease. *Circ. Res.* 93, 292–301. <https://doi.org/10.1161/01.RES.0000087542.26971.D4>.
- Wichmann, A., Allahyar, A., Greiner, T.U., Plovier, H., Lundén, G.O., Larsson, T., Drucker, D.J., Delzenne, N.M., Cani, P.D., and Bäckhed, F. (2013). Microbial modulation of energy availability in the colon regulates intestinal transit. *Cell Host Microbe* 14, 582–590. <https://doi.org/10.1016/j.chom.2013.09.012>.
- Wolf, A.J., Reyes, C.N., Liang, W., Becker, C., Shimada, K., Wheeler, M.L., Cho, H.C., Popescu, N.I., Coggeshall, K.M., Arditi, M., and Underhill, D.M. (2016). Hexokinase Is an Innate Immune Receptor for the Detection of Bacterial Peptidoglycan. *Cell* 166, 624–636. <https://doi.org/10.1016/j.cell.2016.05.076>.
- Wu, R., Wyatt, E., Chawla, K., Tran, M., Ghanefar, M., Laakso, M., Epting, C.L., and Ardehali, H. (2012). Hexokinase II knockdown results in exaggerated cardiac hypertrophy via increased ROS production. *EMBO Mol. Med.* 4, 633–646. <https://doi.org/10.1002/emmm.201200240>.
- Zhu, X., Hogan, S.P., Molkentin, J.D., and Zimmermann, N. (2016). Cyclophilin D regulates necrosis, but not apoptosis, of murine eosinophils. *Am. J. Physiol. Gastrointest. Liver Physiol.* 310, G609–G617. <https://doi.org/10.1152/ajpgi.00389.2015>.
- Zimmermann, J., Kaleta, C., and Waschina, S. (2020). gapseq: Informed prediction of bacterial metabolic pathways and reconstruction of accurate metabolic models. *bioRxiv*. <https://doi.org/10.1101/2020.03.20.000737>.

STAR★METHODS

KEY RESOURCES TABLE

REAGENT or RESOURCE	SOURCE	IDENTIFIER
<b>Antibodies</b>		
Anti-Hexokinase 2 (OT14C5)	Novus Biologicals	Cat# NBP2-02272, RRID:AB_2892669
HRP Anti-beta Actin	Abcam	Cat# ab20272, RRID: AB_445482
Anti-Caspase 3/cCaspase 3	Cell Signaling Technology	Cat# 9542, RRID:AB_2160739
Anti-PARP1/cPARP1	Cell Signaling Technology	Cat# 9662, RRID:AB_331439
Anti-Mouse IgG	TH Geyer	NA931V RRID:AB_772210
Anti-Rabbit	TH Geyer	NA934V RRID:AB_772206
PE CD326 (EpCAM)	Bio legend	Cat# 118206 RRID:AB_1134172
Anti-Ki67	BD Biosciences	Cat# 556003 RRID:AB_396287
<b>Bacterial and virus strains</b>		
Oligo mouse microbiota (OMM) ( <i>Bacterioides caecimuris</i> I48, <i>Muribaculum intestinale</i> YL27, <i>Akkermansia muciphila</i> YL44, <i>Turicimonas muris</i> YL45, <i>Limosilactobacillus reuteri</i> I49, <i>Enterococcus faecalis</i> KB1, <i>Blautia coccoides</i> YL58, <i>Clostridium innocuum</i> I46, <i>Flavonifractor plautii</i> YL31, <i>Enterocloster clostridioforme</i> YL32, <i>Acutalibacter muris</i> KB18 and <i>Bifidobacterium animalis</i> YL2)	Max von Pettenkoffer-Institute, Medical Faculty, Ludwig-Maximilians-University Munich	(Brugiroux et al., 2016)
<i>B. thetaiotaomicron</i> VPI-5482	Edison Family Center for Genome Sciences and Systems Biology, Washington University School of Medicine	(Goodman et al., 2009)
<i>E. coli</i> W3110	Edison Family Center for Genome Sciences and Systems Biology, Washington University School of Medicine	(Karow and Georgopoulos, 1992)
<i>B. longum</i> NCC 2705	Nestlé Research Center, Lausanne, Switzerland	N/A
Altered Schaedler Flora (ASF) (2 Clostridia species ASF356 & ASF502, <i>Lactobacillus murinus</i> ASF361 and spec. ASF360, <i>Mucispirillum schaedleri</i> ASF457, <i>Eubacterium plexicaudatum</i> ASF492, <i>Parabacteroides spec.</i> ASF519 and an unknown Firmicutes bacterium ASF500)	Taconic	Ca# ASF-DONOR (Schaedler et al., 1965)
<b>Biological samples</b>		
Serum and tissue from Hk2 <sup>ΔIEC</sup> mice	This paper	N/A
Serum and tissue from Hk2 <sup>fl/fl</sup> mice	This paper	N/A
<b>Chemicals, peptides, and recombinant proteins</b>		
Dextran sodium sulfate	Sigma-Aldrich	Cat# D8906
Sodium butyrate	Sigma-Aldrich	Cat# B5887
Sodium acetate	Sigma-Aldrich	Cat# S2889
Tributylerin	Sigma-Aldrich	Cat# W222305
Minimal Essential Medium (MEM)	Thermo Fischer Scientific	Cat# 31095-052
Fetal bovine serum (FBS)	Biochrom	Cat# S0115
Advanced Dulbecco's Modified Eagle Medium/Ham's F-12 (DMEM/F-12)	Life Technologies GmbH	Cat# 12634028
Dulbecco's Modified Eagle Medium (DMEM)	Life Technologies GmbH	Cat# 41966-029
Penicillin/streptomycin	Life Technologies GmbH	Cat# 15140-122

(Continued on next page)

**Continued**

REAGENT or RESOURCE	SOURCE	IDENTIFIER
Human recombinant EGF Protein,CF	R&D Systems	Cat# 236-EG
Dulbecco's Phosphate Buffered Saline (DBPS)	Life Technologies GmbH	Cat# 14190136
GlutaMAX	Thermo Fisher / GIBCO	Cat# 35050-038
(4-(2-hydroxyethyl)-1-piperazineethanesulfonic acid) (HEPES)	Sigma-Aldrich	Cat# H3375
Puromycin	Sigma-Aldrich	Cat# P7255
Zeocin	Thermo Fisher	Cat# 46-0509
Ethylenediaminetetraacetic acid (EDTA)	Sigma-Aldrich	Cat# E9884
DL-Dithiothreitol (DTT)	Sigma-Aldrich	Cat# 43815
SYBR Select Master Mix	Applied Biosystems	Cat# 4472920
100x Halt Protease inhibitor cocktail	ThermoFisher Scientific	Cat# 78452
RIPA Lysis and Extraction Buffer	ThermoFisher Scientific	Cat# 89900
BD Matrigel Growth factor reduced, Phenol red free	BD	Cat# 356231
N-Acetylcystein (NAC)	Sigma	A9165-25G
Immun-Blot PVDF Membrane	Biorad	Cat# 162-0177
Blotto, non-fat dry milk	Santa Cruz	Cat# sc-2325
Albumin Fraktion V	Carl Roth	Cat# 8076.4
Acetic acid	Sigma Aldrich	Cat# A6283
Propionic acid	Sigma Aldrich	Cat# P1386
Butyric acid	Sigma Aldrich	Cat# B103500
Tween 20	Carl Roth	Cat# 9127.2
Recombinant human interleukin 17 alpha	Immunotools	Cat#11340170
Recombinant human tumor necrosis factor alpha	InvivoGen	Cat# rcyc-htnfa
Recombinant human interferon beta 1 alpha	Immunotools	Cat#11343520
Mouse tumor necrosis factor-alpha recombinant protein	ThermoFisher	Cat# # PMC3016
D(+)-Glucose	Sigma Aldrich	Cat# G8270
Fluorescein isothiocyanate-dextran (FITC)	TH Geyer	Cat# 46944
Anaerobic Akkermansia Medium (AAM)	(Brugiroux et al., 2016)	N/A
<i>Bacterioides ceacimuris</i> I48 supernatant	This paper	N/A
<i>Muribaculum intestinale</i> YL27 supernatant	This paper	N/A
<i>Akkermansia muciphila</i> YL44 supernatant	This paper	N/A
<i>Turicimonas muris</i> YL45 supernatant	This paper	N/A
<i>Limosilactobacillus reuteri</i> I49 supernatant	This paper	N/A
<i>Enterococcus faecalis</i> KB1 supernatant	This paper	N/A
<i>Blautia coccoides</i> YL58 supernatant	This paper	N/A
<i>Clostridium innocuum</i> I46 supernatant	This paper	N/A
<i>Flavonifractor plautii</i> YL31 supernatant	This paper	N/A
<i>Enterocloster clostridioforme</i> YL32 supernatant	This paper	N/A
<i>Acutalibacter muris</i> KB18 supernatant	This paper	N/A
<i>Bifidobacterium animalis</i> YL2 supernatant	This paper	N/A
(3-Nitrophenyl)-hydrazin -hydrochlorid	Sigma Aldrich	Cat#N21804
Acetonitrile	Merck	Cat# 1.00029.1000
Valproic Acid	Sigma Aldrich	Cat# PHR1061-1G
Methanol	Merck	Cat# 1.06035.1000
Ammonium acetate	Sigma Aldrich	Cat# 9691
Santacruzamate A/ CAY-10683	Hözel (MedChemExpress)	Cat# HY-N0931
RGFP966	Hözel (MedChemExpress)	Cat# HY-13909-10mM

(Continued on next page)

<b>Continued</b>		
REAGENT or RESOURCE	SOURCE	IDENTIFIER
PCI-34051	MedChemExpress	Cat# HY-15224
TC-H 106	MedChemExpress	Cat# HY-19348
Vorinostat SAHA	Sigma Aldrich	Cat# SML0061-25MG
TMP269	MedChemExpress	Cat# HY-18360
$\beta$ -Nicotinamide adenine dinucleotide phosphate sodium salt hydrate	Sigma-Aldrich	Cat# N0505-1G
SIS17	MedChemExpress	Cat# HY-128918
<b>Critical commercial assays</b>		
Lamina Propria Dissociation Kit	Miltenyi Biotec	Cat # 130-097-410
GeneArt® CRISPR Nuclease Vector with CD4 Enrichment Kit	ThermoFisher Scientific/ Life Technologies	Cat # A21175
Dynabeads® CD4 Positive Isolation Kit	Invitrogen	Cat# 11331D
Lipofectamine® 3000 Transfection Reagent	ThermoFisher Scientific	Cat# L3000015
RNeasy Mini Kit	QIAGEN	Cat# ID:74004
Maxima H Minus First Strand cDNA Synthesis Kit	ThermoFisher Scientific	Cat# K1651
TruSeq stranded mRNA Kit	Illumina	Cat# 20020594
DC Protein Assay	Biorad	Cat# 5000111
Murine CXCL1/KC Quantikine	R&D Systems	Cat# MKC00B
Pierce ECL Plus Western Blotting Substrate	Thermo Fisher	CAT# 32132X3
ECL™ Western Blotting Detection Reagents	GE Healthcare UK	Cat# RPN2209
Seahorse XF Cell Mito Stress Test Kit	Aligent	Cat#103015-100
Seahorse XF Glycolysis Stress Test Kit	Aligent	Cat# 103020-100
ApopTag Plus Peroxidase <i>In Situ</i> Apoptosis Detection Kit	Sigma-Aldrich	Cat# S810
Vectastain ABC kit	Vector Laboratories	Cat# PK-4000
NucleoSpin Bead Tubes Type A (50)	Macherey-Nagel	Cat# 740786.50
Haemocult®	Beckman Coulter	Cat# 08438859 No longer available
Accu-Check Inform II	Roche	Cat# 05942861
Viromer Blue Kit for siRNA transfection	Lipocalyx	Cat# VB-01LB-00 Note: No longer available to order
<b>Deposited data</b>		
RNA sequencing data	This paper	NCBI's Sequence Read Archive under the accession number GSE158026.
16S amplicon sequencing data	This paper	European Nucleotide Archive (ENA, <a href="https://www.ebi.ac.uk/ena">https://www.ebi.ac.uk/ena</a> ) under the study accession number PRJEB40281
<b>Experimental models: Cell lines</b>		
Caco2	German Collection of Microorganisms and Cell Cultures	Cat# ACC-169, RRID:CVCL_0025
HK2 deficient Caco2	This paper	N/A
HEK Noggin	(Miyoshi and Stappenbeck, 2013)	N/A
HEK R-Spondin-1	(Miyoshi and Stappenbeck, 2013)	N/A
<b>Experimental models: Organisms/strains</b>		
Hk2 <sup><math>\Delta</math>IEC</sup> mice	This paper	N/A
Hk2 <sup>fl/fl</sup> mice	This paper	N/A
Hk2 <sup>fl/fl</sup> intestinal organoids (WT)	This paper	N/A
Hk2 <sup><math>\Delta</math>IEC</sup> intestinal organoids (KO)	This paper	N/A

(Continued on next page)

**Continued**

REAGENT or RESOURCE	SOURCE	IDENTIFIER
<b>Oligonucleotides</b>		
siGenome siRNA FFAR3 (Human) Smart Pool	Horizon	Cat# 005572-00-0005
siGenome siRNA FFAR2 (Human) Smart Pool	Horizon	Cat#M-005574-00-0005
siGenome siRNA HCAR2 (Human) Smart Pool	Horizon	Cat# M-006688-03-0005
Primers for RT-PCR analysis & CRISPR cloning	This paper	Table S3
<b>Recombinant DNA</b>		
CRISPR plasmid targeting human <i>Hk2</i>	This paper	N/A
<b>Software and algorithms</b>		
Graph-Pad-Prism software, version 9.2	Graphpad	<a href="https://www.graphpad.com">https://www.graphpad.com</a>
Adobe Illustrator Version 25.3	Adobe	<a href="http://www.adobe.com">www.adobe.com</a>
ImageJ bundled with Java 1.8.0_172	ImageJ	<a href="https://imagej.nih.gov/ij/download.html">https://imagej.nih.gov/ij/download.html</a>
BD CellQuest Pro™ Software	Becton Dickinson	<a href="https://www.bd.com">https://www.bd.com</a>
Flowing Software	Perttu Terho, Turku Centre for Biotechnology, Finland	<a href="https://bioscience.fi/services/cell-imaging/flowing-software/">https://bioscience.fi/services/cell-imaging/flowing-software/</a>
ZEN pro	Zeiss	<a href="https://www.zeiss.com">https://www.zeiss.com</a>
Trim Galore, version 0.4.4	Babraham Bioinformatics	<a href="http://www.bioinformatics.babraham.ac.uk/projects/trim_galore/">www.bioinformatics.babraham.ac.uk/projects/trim_galore/</a>
STAR aligner, version 2.5.2b	Alexander Dobin	<a href="https://github.com/alexdobin/STAR">https://github.com/alexdobin/STAR</a>
QuantAnalysis	Bruker, Daltonics, Bremen, Germany	<a href="http://www.bruker.com">www.bruker.com</a>
Tecan-i.control software 1.9	Tecan, Männedorf, Switzerland	<a href="http://www.tecan.com">www.tecan.com</a>
featureCounts (version 1.5.2)	Subreads	<a href="http://subread.sourceforge.net/">http://subread.sourceforge.net/</a>
ChimeraSlayer	N/A	(Haas et al., 2011)
PyNAST	N/A	(Caporaso et al., 2010a)
FastTree 2	N/A	(Price et al., 2010)
DEseq2	N/A	(Love et al., 2014)
gapseq	N/A	(Zimmermann et al., 2020)
Bioconductor package topGO (version 2.32.0)	Bioconductor	<a href="https://bioconductor.org">https://bioconductor.org</a>

**RESOURCE AVAILABILITY****Lead contact**

Further information and requests for resources and reagents should be directed to and will be fulfilled by the Lead Contact: Felix Sommer ([f.sommer@ikmb.uni-kiel.de](mailto:f.sommer@ikmb.uni-kiel.de)).

**Material availability**

All newly generated materials are available from the corresponding author upon reasonable request.

**Data and code availability**

- All data is either included in this manuscript or deposited on public databases. The RNA sequencing data has been deposited at NCBI's Sequence Read Archive under the accession number GSE158026. The 16S amplicon sequencing data are accessible through the European Nucleotide Archive (ENA, <https://www.ebi.ac.uk/ena>) under the study accession number PRJEB40281. Additional data that support the findings of this study are available from the corresponding author upon reasonable request.
- All codes used to generate the bioinformatic analyses are available from the lead author upon reasonable request.
- Any additional information required to reanalyze the data reported in this paper is available from the lead contact upon reasonable request.

**EXPERIMENTAL MODEL AND SUBJECT DETAILS****Animals**

All animal experiments were approved by the local animal safety review board of the federal ministry of Schleswig Holstein and conducted according to national and international laws and policies (V 312-72241.121-33 (95-8/11) and V242-62324/2016 (97-8/16)).

Specific-pathogen free (SPF) C57BL/6j animals were housed in the Central Animal Facility (ZTH) of the University Hospital Schleswig Holstein (UKSH, Kiel, Germany). To create the Hk2<sup>ΔIEC</sup> mouse line, we crossed commercially available mice carrying a floxed *Hk2* allele (EMMA #02074, (Heikkinen et al., 1999)) with mice expressing the CRE recombinase under the control of the *Villin* promoter (all in C57BLj genetic background). As controls we used littermate Hk2<sup>fl/fl</sup> mice, referred to as WT mice. All mice were kept under a 12-h light cycle at 45%–65% relative humidity and 22°C room temperature, and were fed gamma-irradiated diet (V1534, ssniff) *ad libitum*. Mice were killed by cervical dislocation prior to removing tissues for histological and molecular analyses. For basal phenotyping we used 9 to 11 and 86 to 92 weeks old mice. For DSS-induced colitis we used 10 to 14 weeks old male mice. Both genotypes were co-housed throughout the entire experiment. To induce colitis, mice received 1.5% (w/v) dextran sodium sulfate in autoclaved tap water. For the SCFA intervention mice were fed either a control diet, a butyrate-enriched diet or an acetate-containing diet for ten days prior to inducing colitis by administering DSS. The SCFA supplementation was continued throughout the entire experiment. The butyrate-enriched diet consisted of control feed (V1534, ssniff) supplemented with 10% (w/w) of the butyrate-polymer tributyrin (Sigma Aldrich), as this ensures the release of butyrate in the colon after metabolism by the intestinal microbiota instead of its absorption in the proximal small intestine (Egorin et al., 1999; Wichmann et al., 2013). The acetate-enriched diet consisted of control feed but the drinking water was replaced with autoclaved tap water supplemented with 150 mM sodium acetate (Sigma Aldrich), a concentration used successfully in previous studies (Macia et al., 2015; Maslowski et al., 2009). Disease activity was determined by a combination of weight loss (0 = 0%–5%, 1 = 5%–10%, 2 = 10%–15%, 3 = 15%–20% and 4 = > 20%), stool consistency (0 = formed, 1 = formed but soft, 2 = unformed, 4 = diarrhea) and rectal bleeding (0 = negative Haemoccult (Beckman Coulter), 1 = slightly positive Haemoccult, 2 = strongly positive Haemoccult, 3 = visible blood on stool, 4 = rectal bleeding) as previously described (Aden et al., 2018). For oral glucose tolerance testing (oGTT) mice were fasted for 4 h. A solution, containing 20% glucose (Sigma Aldrich) dissolved in sterile filtered tap water, was applied by gavage. Mice received 2 g glucose per kg of body weight at time point 0. The tail vein was punctured to measure blood sugar via a test strip (Roche) at the time points –30, 0, 15, 30, 60 and 120 min before/after gavage as previously described (Sommer et al., 2016).

Mice received 600 mg Fluorescein Isothiocyanate (FITC) (TH Geyer) per kg body weight via gavage 1 h prior to the sacrifice. FITC concentration in serum was measured via Infinite M200 Pro microplate reader (Tecan, Männedorf, Switzerland) using the Tecan-control software 1.9 (Tecan, Männedorf, Switzerland) as previously described (Gupta and Nebreda, 2014).

Gnotobiotic experiments were performed in the animal facilities of either the Experimental Biomedicine (EBM) of Gothenburg or Hannover Medical School (MHH). All animal protocols were approved by the Gothenburg Animal Ethics Committee or by Lower Saxony State Office for Consumer Protection and Food Safety. Gnotobiotic mice were housed as described under standard procedures (Bolsega et al., 2019; Sommer et al., 2014). Mice were kept under a 12-h light cycle and fed autoclaved chow diet *ad libitum* (Labdiet, St Louis, MO, USA). Mono-associated mice were generated by inoculating 12-week-old GF mice with 200 μl of overnight (stationary phase) *in vitro* cultures of *B. thetaiotaomicron*, *E. coli* or *B. longum* by oral gavage and the mice were sacrificed 14 days post colonization. ASF- and OMM-associated mice were generated by co-housing of weaned germ-free mice for four weeks with gnotobiotic donor animals colonized with either ASF or OMM and sacrificed at an age of 12 weeks.

### Bacteria and *in vitro* culture

*B. thetaiotaomicron* VPI-5482 (ATCC 29148, (Goodman et al., 2009)), *E. coli* W3110 (Karow and Georgopoulos, 1992) were kindly provided by Dr. Jeffrey Gordon (Edison Family Center for Genome Sciences and Systems Biology, Washington University School of Medicine, St. Louis, MO 63110, USA), while *B. longum* NCC 2705 was kindly provided by Dr. Stéphane Duboux, Nestlé Research Center, Lausanne, Switzerland. Liquid media (TYG, LB and MRS broth supplemented with 0.05% (w/v) cysteine), for *B. thetaiotaomicron*, *E. coli* and *B. longum*, respectively) were inoculated with single colonies of cultures on agar plates and were grown to the stationary phase overnight in an anaerobic jar at 37°C. ASF is a mix of eight bacteria: two Clostridia species ASF356 & ASF502, *Lactobacillus murinus* ASF361 and *spec.* ASF360, *Mucispirillum schaedleri* ASF457, *Eubacterium plexicaudatum* ASF492, *Parabacteroides spec.* ASF519 and an unknown Firmicutes bacterium ASF500 (Schaedler et al., 1965). ASF colonized mice were purchased from Taconic and inoculated transgenerally by co-housing. OMM (Oligo-Mouse-Microbiota) is a mix of 12 bacteria: *Bacterioides caecimuris* I48, *Muribaculum intestinale* YL27, *Akkermansia municipiphila* YL44, *Turicimonas muris* YL45, *Limosilactobacillus reuteri* I49, *Enterococcus faecalis* KB1, *Blautia coecoides* YL58, *Clostridium innocuum* I46, *Flavonifractor plautii* YL31, *Enterocloster clostridioforme* YL32, *Acutalibacter muris* KB18 and *Bifidobacterium animalis* YL2 (Brugiroux et al., 2016). The OMM was kindly provided by Prof. Bärbel Stecher (Max von Pettenkoffer-Institute, Medical Faculty, Ludwig-Maximilians-University Munich) Bacteria of the OMM consortium were grown in single cultures under anaerobic conditions in Anaerobic Akkermansia Medium (AAM) as previously described (Brugiroux et al., 2016). Briefly, AAM is mainly based on Brain Heart Infusion and Trypticase soy broth and was supplemented with reducing agents under sterile and anaerobic conditions. Cultures of each OMM strain were collected and cells pelleted by centrifugation at maximum speed for 5 min. The cleared supernatants were then sterile filtered using a 0.2 μm filter and then used for 24 h stimulations.

### Culture of Caco-2 cells

Caco-2<sup>WT</sup> and Caco-2<sup>ΔHk2</sup> cells were cultured at 37°C with 5% CO<sub>2</sub> atmosphere in MEM with 20% (v/v) Fetal bovine serum (FBS) purchased from Biochrom. Cells were seeded with 70% confluency and 24 h in advance of stimulation. Cells were stimulated for a period of 24 h. All used stimulant concentrations are listed in the legends of the corresponding figures.

### Culture of intestinal organoids

Intestinal organoids were generated following procedures described earlier by Sato et al., 2009 (Sato et al., 2009). Organoids were cultivated at 37°C with 5% CO<sub>2</sub> atmosphere in 24 well plates in Matrigel (BD) with ENR-conditioned medium supplemented with 0.1% human recombinant EGF (50 µg/mL) as described by Sato et al., 2011 (Sato et al., 2011). ENR-conditioned medium consisted of 70% (v/v) 2x basal medium (Advanced DMEM/F12 supplemented with HEPES [1M], Glutamax [100x], Penicillin/streptomycin 10,000 U/mL [1:50] and N-Acetylcysteine [500 mM]), 10% (v/v) Noggin-conditioned medium and 20% R-Spondin-conditioned medium. Intestinal organoids were stimulated for a period of 24 h. All used stimulant concentrations can be found in the legends of the corresponding figures.

## METHOD DETAILS

### Noggin-conditioned medium

HEK Noggin cells were described previously (Miyoshi and Stappenbeck, 2013) and kindly provided by the group of Prof. Zeissig (CRTD, Dresden University, Germany). Briefly, HEK cells were engineered to secrete Noggin protein into the culture medium. The cells were thawed in DMEM + 10% (v/v) FBS purchased from Biochrom. After reaching confluency, cells were cultured for 3 cycles using DMEM + 10% (v/v) FBS + 10 µg/mL Puromycin (Sigma-Aldrich). After the 3<sup>rd</sup> cycle cells were diluted 1:20 and cultured in DMEM + 10% (v/v) FBS without Puromycin. After 4 days the medium was collected and centrifugated to remove excess cells. New DMEM + 10% (v/v) FBS was added to the cells and 4 days later the second batch was collected and centrifugated to remove excess cells. Collected medium from the first batch was mixed with the second batch.

### R-Spondin-conditioned medium

HEK R-Spondin-1-producing cells were described previously (Miyoshi and Stappenbeck, 2013) and kindly provided by Prof. Zeissig (CRTD, Dresden University, Germany). Briefly, HEK cells were engineered to secrete R-Spondin-1 protein into the culture medium. The cells were thawed in DMEM + 10% (v/v) FBS (Biochrom). After reaching confluency cells were cultured for 3 cycles using DMEM + 10% (v/v) FBS+ 300 µg/mL Zeocin (Thermo Fisher). After the 3<sup>rd</sup> cycle cells were diluted 1:20 and cultured in DMEM + 10% (v/v) FBS without Zeocin. After 4 days the medium was collected and centrifuged to remove excess cells. New DMEM + 10% (v/v) FBS was added to the cells and 4 days later the second batch was collected and centrifuged remove excess cells. Collected medium from the first batch was mixed with the second batch.

### Isolation of primary cells

IECs were isolated from intestinal tissue using the Lamina Propria Dissociation Kit (Miltenyi BioTech, Bergisch Gladbach, Germany) according to the manufacturer's protocol with minor deviations as described before (Pan et al., 2018). In brief, intestinal epithelial cells were isolated by disruption of the structural integrity of the epithelium using ethylenediaminetetraacetic acid (EDTA) and dithiothreitol (DTT). Purity of individual IEC fractions was analyzed by flow cytometry on a FACS Calibur flow cytometer (B&D, Heidelberg, Germany) with Cellquest analysis software from Becton Dickinson. We used the Anti-EpCam-PE (Clone: G8.8, Biolegend, San Diego, USA) antibody for analysis of IEC purity. FACS-data was analyzed using Flowing Software (Perttu Terho, Turku Centre for Biotechnology, Finland).

### Generation and culture of HK2-deficient Caco-2 cells

A CRISPR plasmid targeting human *Hk2* was generated using the GeneArt® CRISPR Nuclease Vector Kit from Thermo Fisher. Caco-2 cells were purchased from DSMZ (ACC-169) and transfected with the *Hk2* CRISPR plasmid using the Lipofectamin 3000 reagent kit (Thermo Fisher Scientific). Positive clones were purified by the Dynabeads® CD4 Positive Isolation Kit (Invitrogen) and screened via western blot to generate a monoclonal population termed Caco-2<sup>ΔHk2</sup>. Caco-2 cells that were also subjected to the CRISPR transfection and selection procedure, but which still showed a HK2 band as per western blot analysis were used as controls (Caco-2<sup>WT</sup>).

### siRNA Transfection

Free Fatty Acid Receptor 3 (FFAR3), Free Fatty Acid Receptor 2 (FFAR2) and Hydroxycarboxylic Acid Receptor 2 (HCAR2) were silenced using small interfering RNA (siRNA). Caco-2 were transfected with siRNA for FFAR3, FFAR2 and HCAR2 or mock siRNA (Horizon) 24 h after seeding using the Viromer Blue Kit for siRNA transfection (Lipocalyx) following the manufacturers instruction. Butyrate (Sigma Aldrich) was added 48 h after siRNA transfection.

### RNA isolation and qPCR

Total RNA was extracted using the RNeasy Mini Kit (QIAGEN) according to the manufacturer's protocol. RNA concentration was measured using a NanoDrop ND-1000 spectrophotometer (PeqLab Biotechnologie). 1 µg of total RNA was reverse transcribed to cDNA using the Maxima H Minus First Strand cDNA Synthesis Kit (ThermoFisher Scientific). qPCR was carried out using SYBR Select Master Mix (Applied Biosystems) according to the manufacturer's instructions on a Viiia 7 Real-Time PCR System (ThermoFisher Scientific). Expression levels were normalized to *Actb* (β-actin). Primer sequences for RT-PCR are listed in Table S3.

## RNA sequencing

Total RNA was extracted as described above from isolated IECs from *Hk2*<sup>ΔIEC</sup> and littermate control mice under untreated conditions and after administering DSS for 3 or 7 days. RNA libraries were prepared using TruSeq stranded mRNA Kit (Illumina) according to manufacturer's instructions. All samples were sequenced using an Illumina NovaSeq 6000 sequencer (Illumina, San Diego, CA) with an average of 23 million paired-end reads (2x 50 bp) at IKMB NGS core facilities. The RNA-seq data was processed using an in-house pipeline (<https://github.com/nf-core/rnaseq>). Briefly, adapters and low-quality bases from the RNA-seq reads were removed using Trim Galore (version 0.4.4). The filtered reads were mapped to the mouse genome (GRCm38) using STAR aligner (version 2.5.2b). Expression counts of the transcripts were estimated using featureCounts (version 1.5.2) and then normalized across samples using the DESeq normalization method. DESeq2 (Love et al., 2014) was used to determine differentially expressed genes. Genes were considered as significant differentially expressed if the adjusted *p* value (Benjamini-Hochberg (BH) multiple test correction method) was less than 0.05. Gene Ontology (GO) enrichment analysis was conducted using the Bioconductor package topGO (version 2.32.0) and a Fisher.elim *p* value (weight algorithm) of 0.05 was used as significance threshold.

## Microbiota analysis

MiSeq 16S amplicon sequence data was analyzed using MacQIIME v1.9.1 (<http://www.wernerlab.org/software/macqiime>, (Caporaso et al., 2010b)) as described previously (Fulde et al., 2018; Sommer et al., 2016). Briefly, all sequencing reads were trimmed keeping only nucleotides with a Phred quality score of at least 20, then paired-end assembled and mapped onto the different samples using the barcode information. Sequences were assigned to operational taxonomic units (OTUs) using uclust and the greengenes reference database (gg\_13\_8 release) with 97% identity (DeSantis et al., 2006; Edgar, 2010). Representative OTUs were picked and taxonomy assigned using uclust and the greengenes database. Quality filtering was performed by removing chimeric sequences using ChimeraSlayer (Haas et al., 2011) and by removing singletons and sequences that failed to align with PyNAST (Caporaso et al., 2010a). The reference phylogenetic tree was constructed using FastTree 2 (Price et al., 2010). All samples within a single analysis were normalized by rarefaction to the minimum shared read count to account for differential sequencing depth among samples (10,174 sequences per sample). Relative abundance was calculated by dividing the number of reads for an OTU by the total number of sequences in the sample. Alpha diversity measures were computed and beta diversity was calculated using Unweighted Unifrac and visualized by principal coordinate analysis. Significance of differences in abundances of various taxonomic units between *Hk2*<sup>ΔIEC</sup> and littermate control mice was calculated using *t* test and *p* values were adjusted for multiple testing using FDR correction (*q*-value).

## Western blot analyses

Caco-2 cells and organoids were lysed using RIPA buffer + 1% Halt Protease inhibitor cocktail (Thermo Fisher Scientific). Lysates were heated to 95°C for 5 min centrifuged at 16,000 g for 15 min at 4°C to remove cell remnants. Protein concentrations were measured by DC Protein Assay (BioRad) according to the manufacturers protocol. Equal amounts of lysates containing Laemmli buffer (250 mM TRIS, 10% (v/v) SDS, 50% (v/v) Glycerol, 500 mM DTT and Bromophenol blue) were heated at 95°C and electrophoresed on 10% or 15% polyacrylamide gels under standard SDS-PAGE conditions before being transferred onto a Immobilon-P Membrane (Biorad). Protein loaded membranes were blocked with 5% (w/v) non-fat dry milk or bovine serum albumin (BSA) in Tris-buffered saline (TBS) (200 mM TRIS, 1.37 M NaCl) supplemented with 0.1% (v/v) Tween 20 for 1 h, incubated with primary antibody (mouse anti-HK2, Novus Biologicals, #NBP2-02272; rabbit anti-PARP1/cPARP1, Cell Signaling Technology, #9542; rabbit anti-Caspase3/cCaspase3, Cell Signaling Technology, #9662, mouse anti-betaActin, Abcam, #ab20272) overnight, washed three times with TBS-Tween-20 and then incubated with the secondary horseradish peroxidase (HRP)-conjugated antibody for 1 h at room temperature. Proteins were detected using the Pierce ECL and ECL Plus Substrate Kits (ThermoFisher).

## Histology and immunostaining

Tissue specimen were fixed in 10% formalin solution over night at 4°C and then embedded in paraffin. 5 μm thick sections were cut and stained with hematoxylin and eosin (H&E) or subjected to immunostaining using the Vectastain ABC kit (Vector Laboratories) including antigen retrieval in boiling citrate buffer. Primary antibodies were incubated overnight. For immunostaining of HK2 we used a 1:1000 diluted antibody (Novus Biologicals, #NBP2-02272). Using ImageJ (version 1.8.0\_172, <https://imagej.nih.gov/ij/index.html>) free hand selection was used to select the HK2 positive colonic epithelium and the intensity of staining was measured using the mean gray value of the pixel area. We calculated the average gray value of 20 selected sections per colon. We then subtracted the average Grey Scale value of from the background white (255- sample average). We used the mean gray value of all chow treated WT mice (Basal phenotyping) and set it to 100% to compare the intensity to the chow WT mice. For immunostaining of Ki67 we used a 1:500 diluted mouse anti-Ki67 antibody (BD Biosciences, cat.no. 556003). The TUNEL assay was performed using the ApopTag Plus Peroxidase *In Situ* Apoptosis Detection Kit (Merck Millipore) according to the manufacturer's instructions. Slides were visualized using a Zeiss Imager Z1 microscope (Zeiss) and pictures were taken using ZEN pro (Zeiss) software. Histological disease activity was assessed in a blinded fashion as previously described (Siegmond et al., 2001). Briefly, the scoring is calculated as a combined score of inflammatory cell infiltration and tissue damage.

### Seahorse analysis

To perform real-time ECAR and OCR-analyses, Caco-2 cells were analyzed using the Seahorse XF24 Analyzer from Agilent Technologies by Mito Stress Test Kit or Glycolysis Stress Test Kit according to the manufacturer's instructions.  $4 \times 10^4$  cells were used in each assay with  $n = 9$  replicates in three independent experiments. Cells were seeded 24 h prior to the assay. To study the effect of butyrate the assay was conducted after 48 h to allow a 24 h stimulation with 2mM butyrate (Sigma Aldrich).

### Metabolic modeling of SCFA production by OMM bacteria

Metabolic networks were reconstructed using gapseq (Zimmermann et al., 2020) based on the genomes of OMM bacteria, which were downloaded from NCBI bioproject PRJNA289613, and the Anaerobic Akkermansia Medium (Brugiroux et al., 2016). The formation of fermentation products was determined via an extended flux balance analysis that minimizes the total flux through all reactions as a proxy for the parsimonious enzyme usage (Lewis et al., 2010). The variability of predictions was taken into account by randomly sampling the space of alternative optimal solutions via the function ACHR from the R package sybilcycleFreeFlux ( $W = 5000$ ,  $nPoints = 10000$ ) (Desouki et al., 2015) to derive the distribution of fermentation products for each bacteria. All predicted fermentation products were then used as explanatory variables to estimate the *Hk2* expression via linear regression.

### Quantification of SCFAs

OMM bacteria were grown as described above and 1 mL of each bacterial culture supernatant was homogenized using NucleoSpin Bead Tubes (Macherey-Nagel, Düren, Germany) and a Precellys Evolution Homogenizer (Bertin Corp., Rockville, Maryland, USA). Homogenates were cleared by centrifugation for 10 min at  $21,000 \times g$  and  $4^\circ\text{C}$ . SCFA standards including acetic, propionic and butyric acid (purchased from Sigma Aldrich, St Louis, MO, USA) were prepared in methanol to a concentration of 100 ppm. Derivatization of SCFAs was performed with 3-nitrophenylhydrazine as described (Liebisch et al., 2019). SCFA concentrations in the samples were then measured via Ultra-High Performance Liquid Chromatography (Acquity UPLC, Waters, Milford, MA, USA) coupled to Mass Spectrometry (amaZon ETD IonTrap, Bruker Daltonics GmbH, Bremen, Germany). Sample separation was performed using a C8 column and solvent system consisting of ammonium acetate (5 mM, Sigma Aldrich, St Louis, MO, USA) combined with acetic acid (0.1%, pH 4.2, Biosolve, Valkenswaard, Netherlands) in water or acetonitrile (LC-MS CHROMASOLV, FLUKA, Sigma Aldrich, St Louis, MO, USA). Mass spectrometry analysis was performed in negative electrospray ionization mode. Peak areas and concentrations of SCFAs in the bacterial supernatants were calculated using QuantAnalysis (Bruker, Daltonics, Bremen, Germany) software.

### ELISA

Enzyme linked immunosorbent assay (ELISA) was used to detect cytokine levels of serum of mice. For measurement of murine CXCL1/KC we used the Murine CXCL1/KC Quantikine (R&D Systems), following the manufacturers protocol. The plates were coated overnight with an antigen-specific capture antibody at room temperature. Afterward the plates were washed with 0,05% Tween 20 in DBPS and blocked using 1% BSA in DBPS. Streptavidin-bound horse radish peroxidase antibody was used as secondary antibody following the manufacturers protocol. The absorbance was measured with an Infinite M200 Pro microplate reader (Tecan, Männedorf, Switzerland) using the Tecan-i.control software 1.9 (Tecan, Männedorf, Switzerland)

### QUANTIFICATION AND STATISTICAL ANALYSIS

Biostatistical analyses were performed using GraphPad Prism (version 8) software (GraphPad, Inc, La Jolla, CA), MacQIIME v1.9.2 or R (v 3.2.5) including data distribution analyses. Data from two groups was assessed for significance using Mann-Whitney U-test, whereas data from multiple groups was analyzed using either one-way or two-way ANOVA. Specific comparisons and analyses are described in the individual method sections. Differences between the groups were considered significant at  $p < 0.05$  and the data are presented as means  $\pm$  SEM.

## Supplemental information

### Microbial regulation of hexokinase 2 links

#### mitochondrial metabolism and cell death in colitis

Finn Hinrichsen, Jacob Hamm, Magdalena Westermann, Lena Schröder, Kensuke Shima, Neha Mishra, Alesia Walker, Nina Sommer, Kenneth Klischies, Daniela Prasse, Johannes Zimmermann, Sina Kaiser, Dora Bordon, Antonella Fazio, Georgios Marinos, Georg Laue, Simon Imm, Valentina Tremaroli, Marijana Basic, Robert Häslar, Ruth A. Schmitz, Stefan Krautwald, Andrea Wolf, Bärbel Stecher, Philippe Schmitt-Kopplin, Christoph Kaleta, Jan Rupp, Fredrik Bäckhed, Philip Rosenstiel, and Felix Sommer

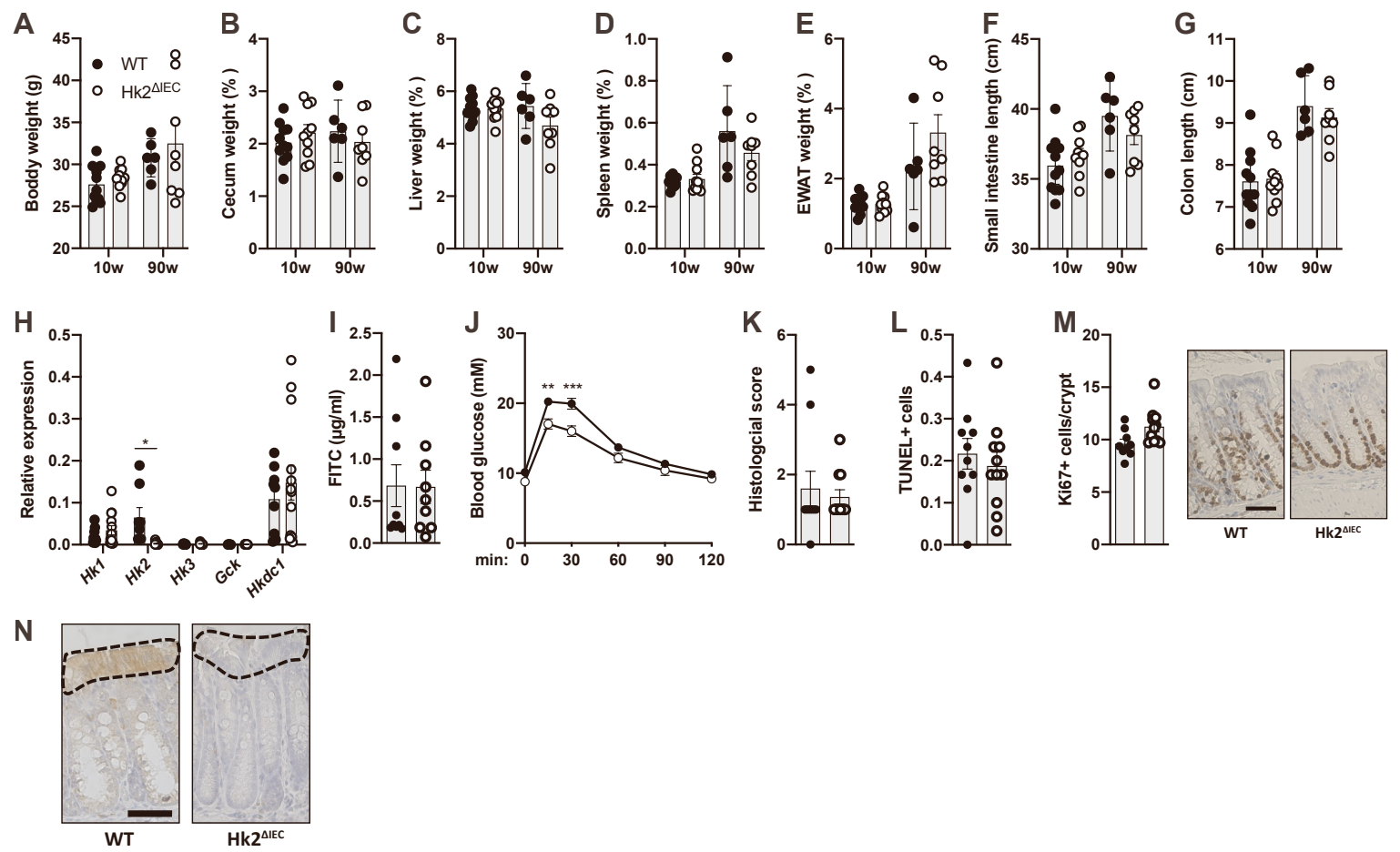


Fig.S1

**Figure S1, related to Figure 1: *Hk2*<sup>ΔIEC</sup> mice do not display an evident immunological or metabolic phenotype under baseline conditions. A-G)** 10- or 90-week-old WT and *Hk2*<sup>ΔIEC</sup> mice were sacrificed and organ measures taken. **A)** Body weight. **B)** Cecum weight. **C)** Liver weight. **D)** Spleen weight. **E)** Epididymal white adipose tissue (EWAT) weight. **F)** Small intestine length. **G)** Colon length. **H)** Relative expression of all hexokinase family members in unfractionated colon tissue of 10-week-old WT and *Hk2*<sup>ΔIEC</sup> mice as per qPCR. **I)** Intestinal permeability as measured by fluorescein isothiocyanate (FITC) levels in blood of 10-week-old WT and *Hk2*<sup>ΔIEC</sup> mice 1h after oral gavage. **J)** Blood glucose levels during oral glucose tolerance test in 10-week-old WT and *Hk2*<sup>ΔIEC</sup> mice. **K)** Colonic histological score of 10-week-old WT and *Hk2*<sup>ΔIEC</sup> mice. **L)** TUNEL-positive cells per colon crypt of 10-week-old WT and *Hk2*<sup>ΔIEC</sup> mice. **M)** Ki-67-positive cells per colon crypt of 10-week-old WT and *Hk2*<sup>ΔIEC</sup> mice including representative images. The scale bar represents 50 μm. **N)** Expression pattern of the HK2 protein in the colonic epithelium of untreated 10-week-old WT and *Hk2*<sup>ΔIEC</sup> mice. The scale bar represents 50 μm. The dotted line indicates the tip epithelium area used for quantification of HK2 protein expression. Note the dominant HK2 expression in the colonic tip epithelium.

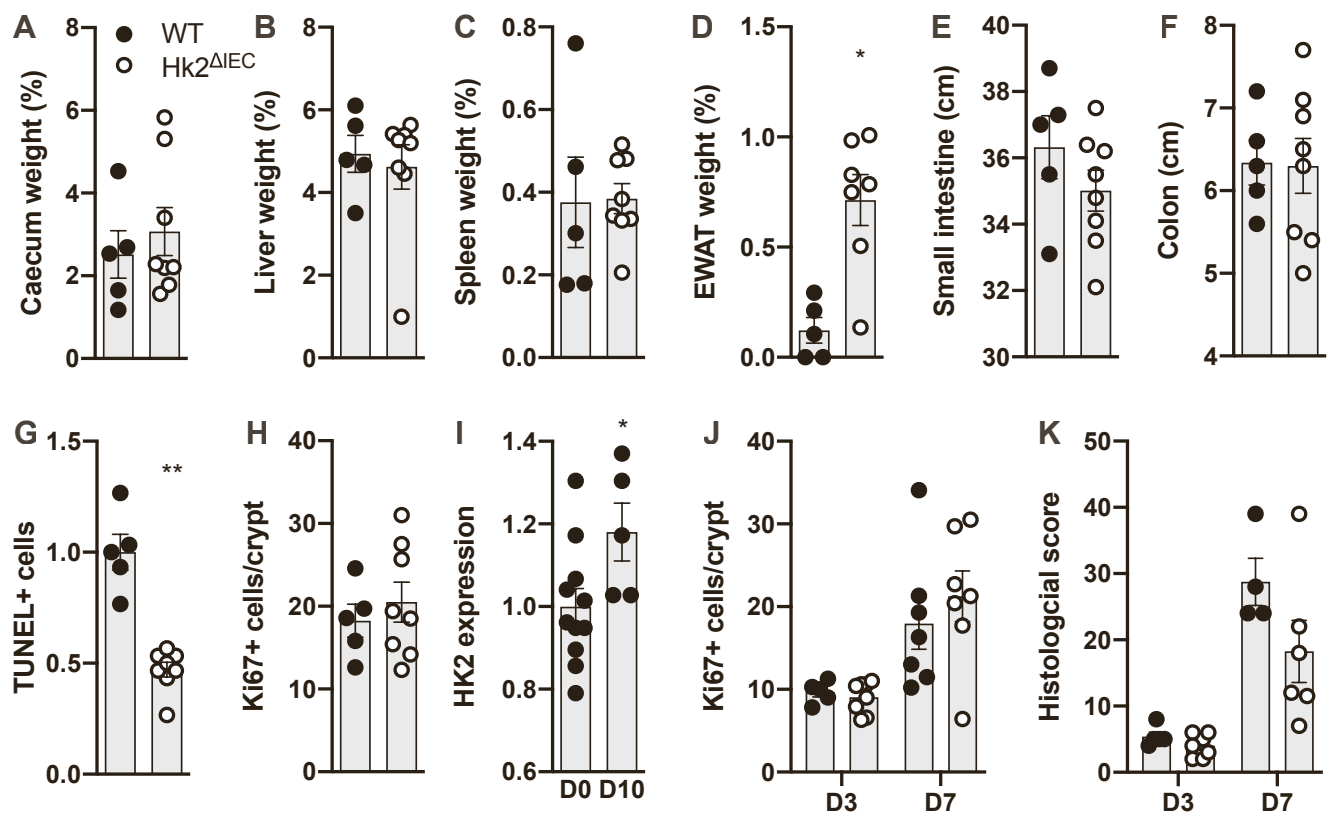
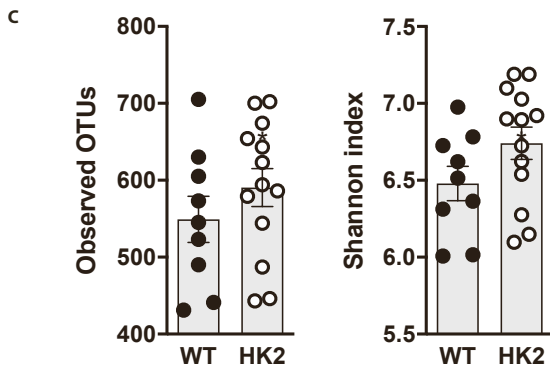
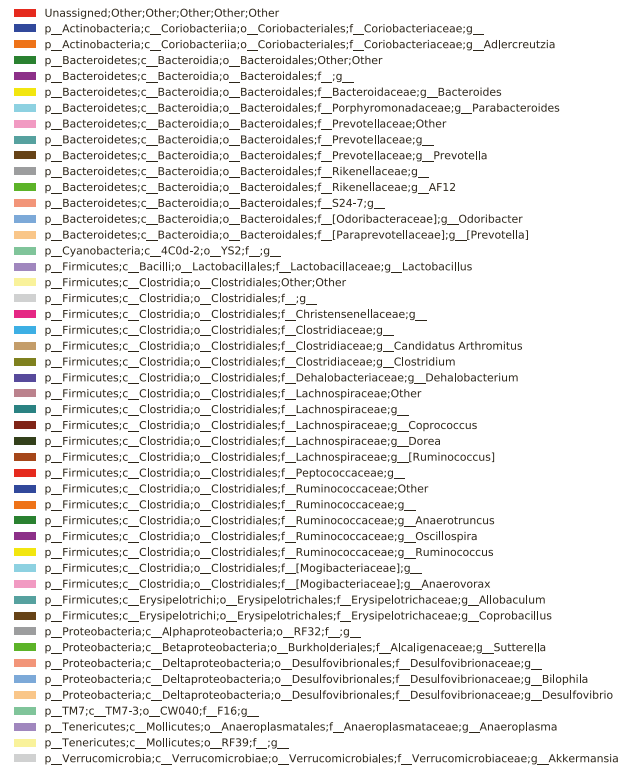
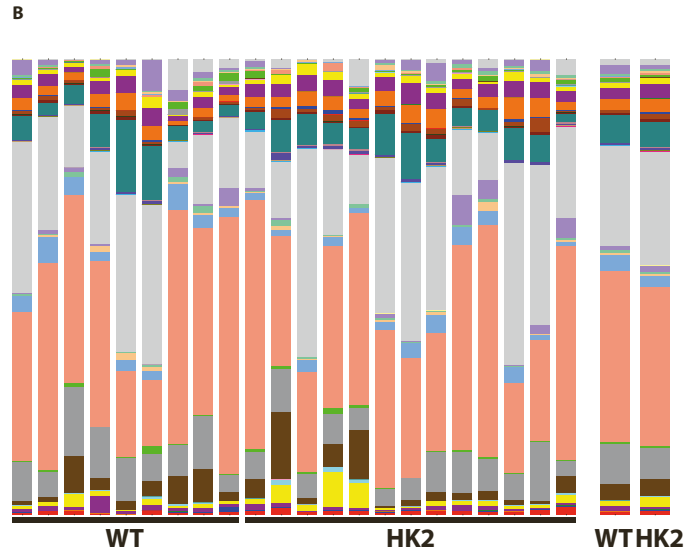
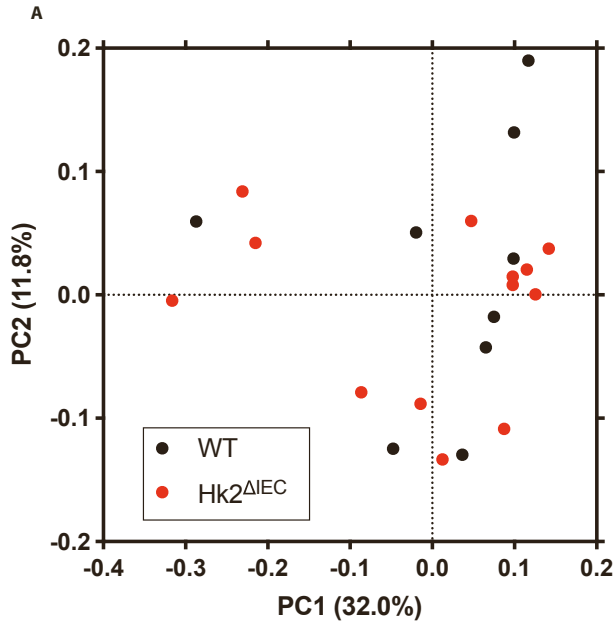


Fig.S2

**Figure S2, related to Figure 1: Phenotyping of WT and *Hk2*<sup>ΔIEC</sup> mice during DSS-induced colitis. A-H)** Organ and histological data from WT and *Hk2*<sup>ΔIEC</sup> mice sacrificed at the end (day 10) of DSS colitis. **A)** Cecum weight. **B)** Liver weight. **C)** Spleen weight. **D)** Epididymal white adipose tissue (EWAT) weight. **E)** Small intestine length. **F)** Colon length. **G)** TUNEL-positive cells per colon crypt. **h)** Ki-67-positive cells per colon crypt. **I)** HK2 protein levels in colon epithelium of WT mice at baseline (day 0) and at day 10 during DSS colitis as determined per immunohistochemistry. **J)** Ki-67-positive cells per colon crypt and **K)** histological score of WT and *Hk2*<sup>ΔIEC</sup> mice at day 3 and 7 during DSS colitis.



**Figure S3, related to Figure 1: Heatmap of genes differentially expressed in colon of WT and *Hk2*<sup>ΔIEC</sup> mice at days 0, 3 and 7 during DSS colitis.** WT and *Hk2*<sup>ΔIEC</sup> mice were given 2% DSS in drinking water and analyzed on day 0, 3 and 7 of treatment. RNA was isolated from unfractionated colon and sequenced to identify transcripts with differential expression dependent on the loss of epithelial HK2 during the onset of inflammation.



**Figure S4, related to Figure 1: Ablation of HK2 in IECs does not alter the composition of the intestinal microbiota. A)** Principal coordinate analysis of fecal microbiota from WT and *Hk2*<sup>ΔIEC</sup> mice. **B)** Taxonomic overview on genus level. **C)** Alpha diversity (the variation of microorganisms in a single sample).

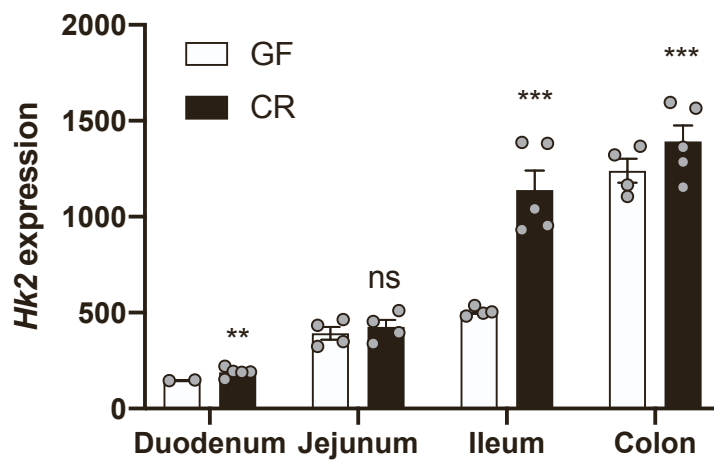


**Figure S5, related to Figure 3: *Hk2* expression increases along the intestinal tract.** *Hk2* expression was determined in whole tissue specimen collected along the length of the intestinal tract of adult C57BL6/J GF and CR mice. Data from (Larsson et al., 2012). n=4-5 per group. \*\* p<0.01 and \*\*\* p<0.001.

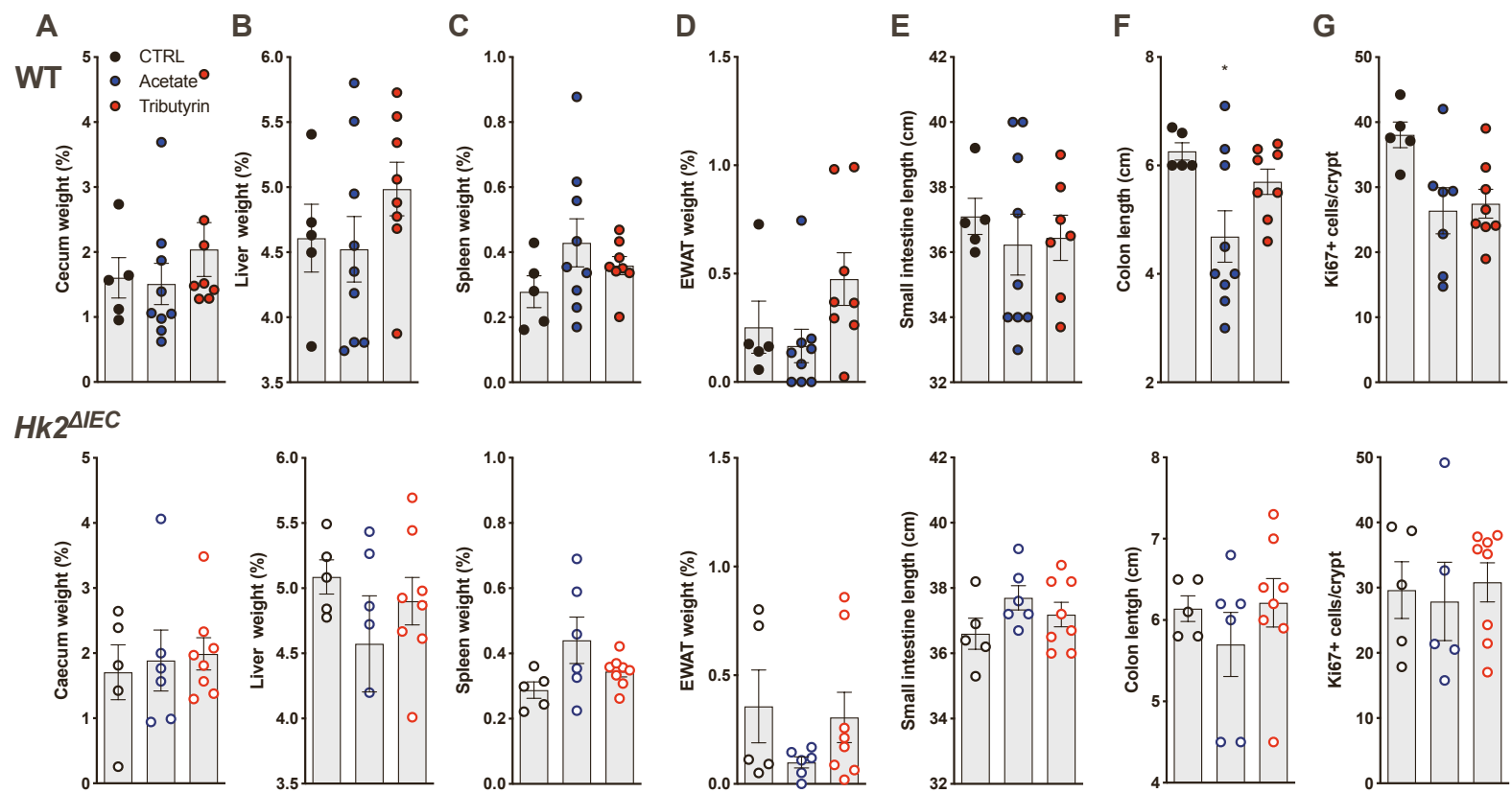


Fig.S6

**Figure S6, related to Figure 4: Organ measures and histological data of WT and *Hk2*<sup>ΔIEC</sup> mice at the end of the dietary SCFA supplementation and DSS-induced colitis experiment. A) Cecum weight. B) Liver weight. C) Spleen weight. D) Epididymal white adipose tissue (EWAT) weight. E) Small intestine length. F) Colon length. G) Ki-67-positive cells per colon crypt.**

**Table S2, related to Figure 3: Statistics of linear modelling of *Hk2* expression induced by metabolites produced by single OMM bacteria grown *in vitro*.** AIC = Akaike Information Criteria. Sigma = standard deviation of the residuals. R<sup>2</sup> = coefficient of determination, referring to the proportion of variance in the dependent variable that is predictable from independent variables. R = Pearson correlation coefficient of predicted metabolite production with *Hk2* expression data.

<b>Formula</b>	<b>AIC</b>	<b>sigma</b>	<b>R2</b>	<b>R</b>	<b>pval</b>
<b>Acetate</b>	-5.1809804	0.16092295	0.19156729	0.43768401	0.17820082
<b>Butyrate</b>	-5.5801726	0.15802932	0.22037951	0.46944596	0.14517284
<b>Propionate</b>	-2.8925022	0.17856407	0.00460373	0.06785081	0.84287465
<b>Acetate &amp; butyrate</b>	-8.0040261	0.13381316	0.56522852	0.75181681	0.00762065

**Table S3, related to STAR Methods: List of primers used in this study.**

Sequence 5'-->3'	Gene	Organism	For/Rev	Purpose	Primer name
CATGTACGTTGCTATCCAGGC	Actb	Human	F	qPCR	807_hActin_(s)qPCR_2_F
CTCCTTAATGTCACGCACGAT	Actb	Human	R	qPCR	808_hActin_(s)qPCR_2_R
CCCCTTGTAAGCCCAAGATC	Rpl32	Human	F	qPCR	3334_Hs-L32_F
TCTGGGTTTCCGCCAGTTA	Rpl32	Human	R	qPCR	3335-Hs_L32-R
AAGGCTTCAAGGCATCTG	Hk2	Human	F	qPCR	3491_hs_Hk2_F
CCACAGGTCATCATAGTTCC	Hk2	Human	R	qPCR	3492_hs_Hk2_R
CTGCTGGTGAAAATCCGTAGTGG	Hk1	Human	F	qPCR	3730_Hs_HK1_F
GTCCAAGAAGTCAGAGATGCAGG	Hk1	Human	R	qPCR	3731_Hs_HK1_R
GTGAGGTTGGGCTAGTTGTAGA	Hk3	Human	F	qPCR	3732_Hs_HK3_F
GTCCAGGGTATGGTCAAGGT	Hk3	Human	R	qPCR	3733_Hs_HK3_R
GAATGACACGGTGGCCACGATG	Gck	Human	F	qPCR	3734_Hs_GCK_F
CACTCGGTATTGACGCACATGCG	Gck	Human	R	qPCR	3735_Hs_GCK_R
GGCTTACATTCTCATTTCC	Hkdc1	Human	F	qPCR	3512_hs_Hkdc1_F
TGTTGCTGCCTGTTCTCTG	Hkdc1	Human	R	qPCR	3513_hs_Hkdc1_R
TTCGGCTACAAAGGCTCCAC	Ppif	Human	F	qPCR	3740_Hs_Ppif_F
TGTGCCATTGTGGTTGGTGA	Ppif	Human	R	qPCR	3741_Hs_Ppif_R
GTAGCTAACACAAGTCCAGTCCT	Ffar2	Human	F	qPCR	3896_Ffar2_F
CTAGGTGTTGCTTTGAAGCTTGT	Ffar2	Human	R	qPCR	3897_Ffar2_R
CTAAGGGTATGCGCGCTAAAG	Ffar3	Human	F	qPCR	3898_Ffar3_F
AGCCCAATCCATAGTGTGTGG	Ffar3	Human	R	qPCR	3899_Ffar3_R
ATGTTGGCTATGAACCGCCAG	Hcar2	Human	F	qPCR	3900_Hcar2_F
GCTGCTGTCCGATTGGAGA	Hcar2	Human	R	qPCR	3901_Hcar2_R
TAAGCGTTCCGCAAGGAGAGTTTT	Hk2	Human	F	CRISPR	3608_Hk2_CRIS_F
TTCCTTGCGGAACCGCTTACGGTG	Hk2	Human	R	CRISPR	3609_Hk2_CRIS_R
GGCTGTATCCCCTCCATCG	Actb	Mouse	F	qPCR	3172_b-actin_F
CCAGTTGGTAACAATGCCATGT	Actb	Mouse	R	qPCR	3173_b-actin_R
CCTCTGGTGAAGCCCAAGATC	Rpl32	Mouse	F	qPCR	2664_L32-F
TCTGGGTTTCCGCCAGTTT	Rpl32	Mouse	R	qPCR	2665_L32-R
CCCTGTGAAGATGTTGCCACT	Hk2	Mouse	F	qPCR	3477_Hk2_F
CCTTCGCTTGCCATTACGCACG	Hk2	Mouse	R	qPCR	3478_Hk2_R
CGGAATGGGGAGCCTTTGG	Hk1	Mouse	F	qPCR	3479_Hk1_F1
GCCTTCCTTATCCGTTTCAATGG	Hk1	Mouse	R	qPCR	3480_Hk1_R1
TGCTGCCACATACGTGAG	Hk3	Mouse	F	qPCR	3483_Hk3_F
GCCTGTCAGTGTACCACAA	Hk3	Mouse	R	qPCR	3484_Hk3_R
GAGATGGATGTGGTGGCAAT	Gck	Mouse	F	qPCR	3485_Gck(Hk4)_F
ACCAGCTCCACATTCTGCAT	Gck	Mouse	R	qPCR	3486_Gck(Hk4)_R
ATGTTTGCAGTACACTTGGTGG	Hkdc1	Mouse	F	qPCR	3489_Hkdc1_F
AGGGTCTCATCCGAGAGCC	Hkdc1	Mouse	R	qPCR	3490_Hkdc1_R
TGGCTCTCAGTTCTTTATCTGC	Ppif	Mouse	F	qPCR	3738_Mm_Ppif_F
ACATCCATGCCCTCTTTGAC	Ppif	Mouse	R	qPCR	3739_Mm_Ppif_R